batteries

MDPI

Review

Research Progress on Iron-Based Materials for Aqueous Sodium-Ion Batteries

Songyang Chang [1], Shen Qiu [1], Swati Katiyar [1], Jose Fernando Florez Gomez [2], Zhenxing Feng [3,*] and Xianyong Wu [1,*]

[1] Department of Chemistry, University of Puerto Rico, Rio Piedras Campus, San Juan, PR 00925, USA
[2] Department of Physics, University of Puerto Rico, Rio Piedras Campus, San Juan, PR 00925, USA
[3] School of Chemical, Biological, and Environmental Engineering, Oregon State University, Corvallis, OR 97331, USA
* Correspondence: zhenxing.feng@oregonstate.edu (Z.F.); xianyong.wu@upr.edu (X.W.)

Abstract: Aqueous sodium-ion batteries (ASIBs) represent a promising battery technology for stationary energy storage, due to their attractive merits of low cost, high abundance, and inherent safety. Recently, a variety of advanced cathode, anode, and electrolyte materials have been developed for ASIBs, which not only enhance our fundamental understanding of the Na insertion mechanism, but also facilitate the research and development of practical ASIB systems. Among these electrode materials, iron-based materials are of particular importance because of the high abundance, low price, and low toxicity of Fe elements. However, to our knowledge, there are no review papers that specifically discuss the properties of Fe-based materials for ASIBs yet. In this review, we present the recent research progress on Fe-based cathode/anode materials, which include polyanionic compounds, Prussian blue, oxides, carbides, and selenides. We also discuss the research efforts to build Fe-based ASIB full cells. Lastly, we share our perspectives on the key challenges that need to be addressed and suggest alternative directions for aqueous Na-ion batteries. We hope this review paper can promote more research efforts on the development of low-cost and low-toxicity materials for aqueous battery applications.

Keywords: aqueous sodium-ion batteries; iron-based materials; cathode; anode; full cells

Citation: Chang, S.; Qiu, S.; Katiyar, S.; Florez Gomez, J.F.; Feng, Z.; Wu, X. Research Progress on Iron-Based Materials for Aqueous Sodium-Ion Batteries. *Batteries* **2023**, *9*, 349. https://doi.org/10.3390/batteries9070349

Academic Editor: Claudio Gerbaldi

Received: 24 May 2023
Revised: 27 June 2023
Accepted: 28 June 2023
Published: 30 June 2023

1. Introduction

The storage of renewable energy sources (solar and wind) requires the development of a low-cost, long-cycling, and high-safety battery system [1,2]. Currently, lithium-ion batteries (LIBs) demonstrate immense success in portable electronics and electric vehicles, and they have also been actively studied for stationary energy storage [3,4]. However, the intrinsically low lithium abundance (~20 ppm) in Earth's crust and the uneven Li distribution concurrently contribute to a high battery cost [5,6], making them unaffordable for grid-scale energy storage. Additionally, the LIB electrolyte is based on the use of volatile and flammable carbonate solvents [7], which brings about safety concerns. Therefore, it is indispensable to develop an alternative battery system that can better satisfy the demands of grid-scale energy storage.

Since the 2010s, sodium-ion batteries (SIBs) have attracted considerable attention as an alternative to LIBs for large-scale energy storage, due to Na's much higher elemental abundance (~23,000 ppm), ubiquitous distribution, and potentially lower cost [8–12]. Although the large Na^+ ion radius (1.02 Å vs. 0.76 Å of Li^+) caused some difficulties in early-stage SIB exploration [13–16], extensive investigations from worldwide researchers have successfully identified promising materials for near-future commercialization. Layered metal oxides [17–19], Prussian blue [20–22], and phosphates [23–25] are three leading cathode materials, and hard carbon is the most promising anode candidate [26–29]. There are several excellent review papers that discuss the prospects and challenges of the commercialization of SIBs [30–33], and readers can refer to these articles for more information. Despite the essential research progress, non-aqueous SIBs still rely on volatile and flammable carbonate electrolytes, which have similar safety concerns to LIBs [34]. Moreover, it remains questionable that non-aqueous SIBs offer a competitive levelized energy cost compared with lead-acid batteries [10], particularly when we consider the use of $NaPF_6$ salts, carbonate solvents, and dry room assembly conditions for SIBs.

Due to these limitations of SIBs, there is a parallel interest in developing aqueous sodium-ion batteries (ASIBs), because of the cost-effective and non-flammable nature of aqueous electrolytes [35,36]. Furthermore, cheap and common salts could be used to make electrolytes, such as sodium sulfate, sodium nitrate, or even sodium chloride [22,37]. Additionally, ASIBs can be manufactured in ambient conditions, which eliminates the need to build or use dry rooms. Therefore, ASIBs exhibit a lower cost and higher safety than non-aqueous SIBs, which are more attractive for stationary energy storage. Figure 1a shows the "rocking-chair" working mechanism of ASIBs, where two insertion compounds serve as the cathode and anode in an aqueous Na-ion electrolyte. During the charge process, the cathode loses electrons and releases Na^+ ions, whereas the anode receives electrons and hosts Na^+ ions. The discharge process is the reverse of this.

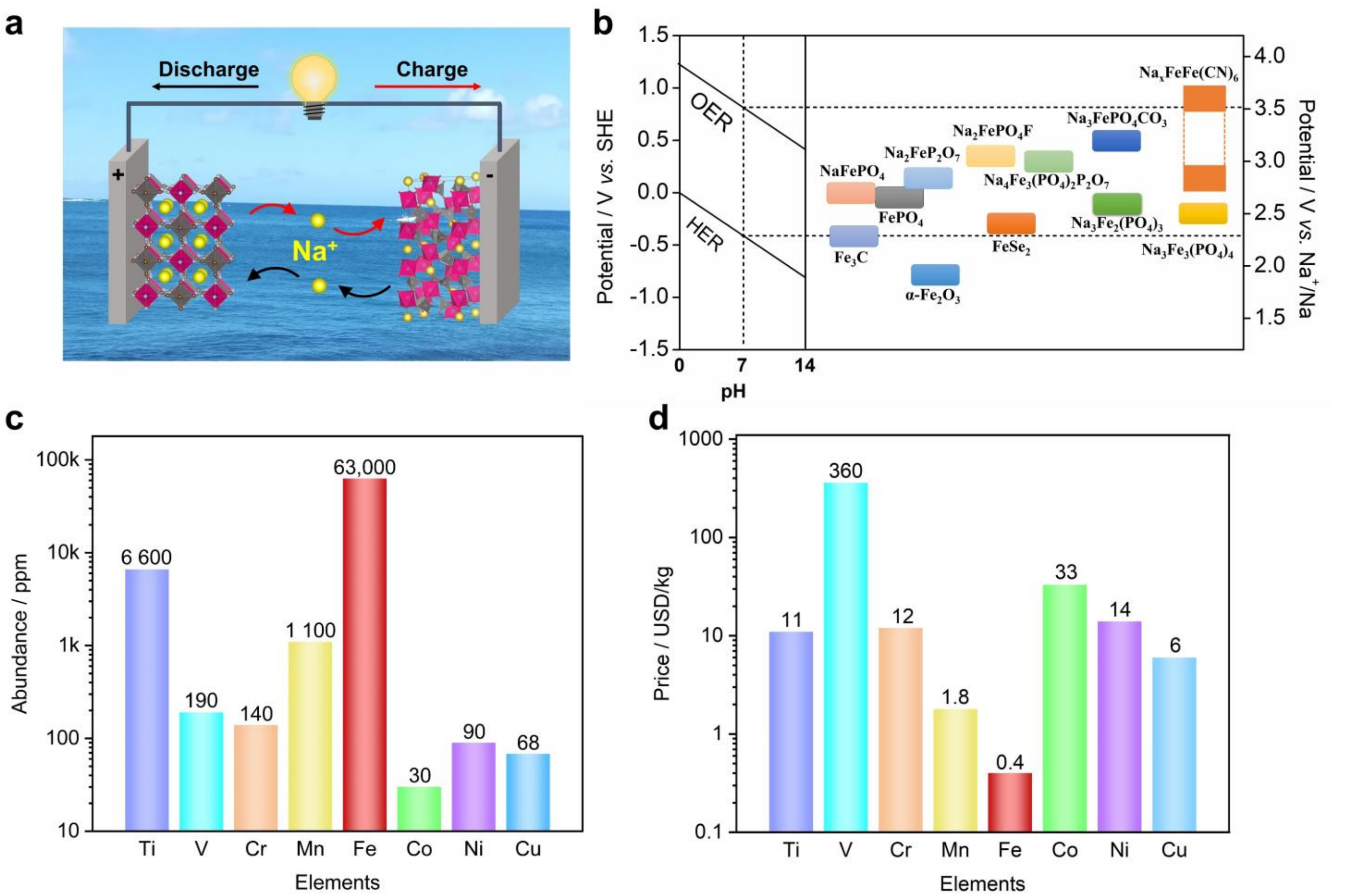

Figure 1. (**a**) The "rocking−chair" working mechanism of aqueous sodium−ion batteries, where two insertion electrode materials serve as the cathode and anode, and the electrolyte is an aqueous Na−ion solution; (**b**) the reaction potentials of Fe−based materials in aqueous electrolytes, with a reference to non−aqueous systems; (**c**) the elemental abundance of transition metals in Earth's crust; (**d**) the elemental price of transition metals. The data were retrieved from the Wikipedia webpage.

Compared with non-aqueous electrolytes, aqueous electrolytes generally have a much narrower electrochemical window, due to the oxidative and reductive decomposition of water molecules, i.e., oxygen evolution reactions (OERs) and hydrogen evolution reactions

(HERs). [38] The thermodynamically stable electrochemical window of water is 1.23 V (Figure 1b), where OER and HER take place at a relative potential of 1.23–0.059 × pH and −0.059 × pH vs. standard hydrogen electrodes (SHEs), respectively. [39] For instance, ina neutral state (pH = 7), OERs and HERs tend to happen at +0.817 V and −0.413 V vs. SHEs, which corresponds to 3.53 V and 2.3 V vs. Na^+/Na, respectively. Note that the Na^+/Na redox couple exhibits a relative potential of −2.713 V vs. SHE. Therefore, researchers could screen suitable electrode materials from a non-aqueous SIB database and apply them to ASIBs. We need to point out that, in practical conditions, aqueous electrolytes support a wider window of 1.5–1.8 V, due to the overpotential contributions from OER and HER [40]. Recently, researchers have worked to increase the salt/solvent ratio and proposed the concept of concentrated or "water-in-salt" (WiS) electrolytes [41–44], which further enlarges the electrolyte window to 2–3.0 V. For instance, Hu et al. reported an inert-cation-assisted WiS electrolyte, which comprises tetraethylammonium (TEA^+) inert cations and Na^+ cations [42]. The very high ion concentration of 31 mol kg^{-1} enabled a broad window of 3.3 V, which supported the functioning of a new anode ($NaTiOPO_4$). Moreover, the Na-ion full cell reached a 1.74 V voltage and high energy of 71 Wh kg^{-1}. Very recently, Wang et al. demonstrated a $NaClO_4$/NaOTF (17 + 2 mol kg^{-1}) bi-salt WiS electrolyte, which can expand the electrochemical window to 4.4 V [45]. This electrolyte can effectively suppress the material dissolution of $Na_3V_2(PO_4)_3$, and the symmetrical $Na_3V_2(PO_4)_3||Na_3V_2(PO_4)_3$ full cell demonstrated a voltage of 1.75 V and an energy density of 70 Wh kg^{-1}. These new electrolytes not only enable more electrode materials to work for ASIBs, but also effectively increase the full cell voltage and energy density.

Compared with other aqueous batteries, such as Ca^{2+}, Mg^{2+}, Al^{3+}, K^+, and NH_4^+ ions, [46–50] ASIBs have the advantages of abundant electrode material choices, which are facilitated by the moderate Na^+ size and the monovalent cation charge. The bulk size of K^+ and NH_4^+ limits the cation insertion to electrode structures, while the high charge density of Ca^{2+}, Mg^{2+}, and Al^{3+} restricts the cation diffusion process. Due to these advantages, the commercialization of ASIBs was attempted by Aquion Energy between 2008 and 2017 [51], which further highlights the attractive merits of ASIBs. To date, a variety of electrode materials have been investigated for ASIBs, including metal oxides [52,53], metal phosphates [54,55], metal hexacyanoferrates (Prussian blue analogues) [56,57], and other compounds [58]. In general, these materials possess one or more transition metal elements for redox reactions, such as titanium, vanadium, chromium, manganese, iron, cobalt, nickel, and copper. Among these materials, iron-based ones are of particular importance for ASIBs, because Fe is the most abundant element (50,000 ppm, Figure 1c) and the most cost-effective element (0.4 USD/kg, Figure 1d) [59,60]. Moreover, Fe-based materials are generally non-toxic or low-toxicity, and are thus vastly different from chromium, vanadium, or cobalt-based materials [61]. Additionally, the Fe element exhibits multiple valance states of +2, +3, and +4 [62], and could be utilized for both cathode and anode reactions, depending on the materials or crystal structures. Based on these discussions, it is appealing to demonstrate Fe-based ASIBs for sustainable energy storage. Nevertheless, there are no review papers on this topic yet.

In this review, we summarize the research progress on Fe-based cathode and anode materials for ASIBs(Figure 2). We talk about the synthesis methods, crystal structures, reaction mechanisms, and electrochemical properties of these materials, and we point out some research limitations, as well. The recent efforts to assemble Fe-based aqueous Na-ion full cells are also discussed. Lastly, we share our perspectives on the key challenges in Fe-based materials and suggest some feasible solutions to overcome these challenges. This review paper will evoke more research interest in the use of Fe-based materials for aqueous batteries and sustainable energy storage.

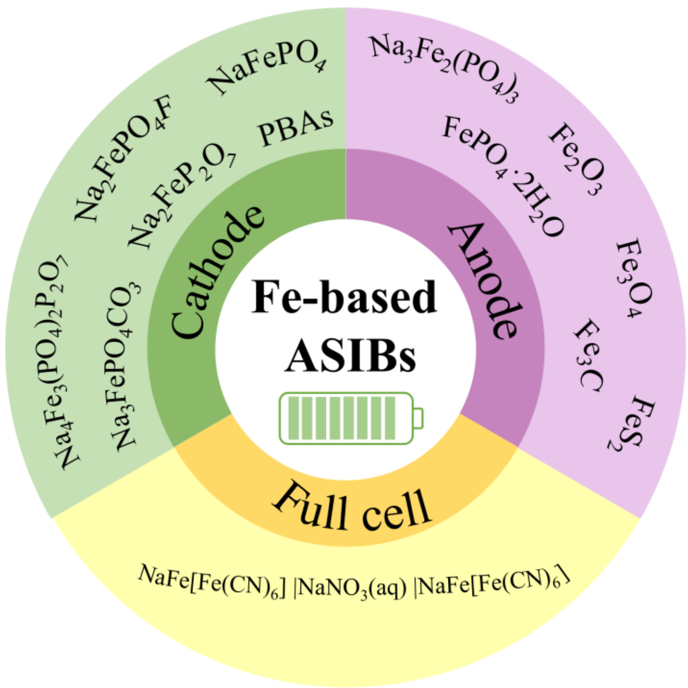

Figure 2. Fe-based cathode, anode, and full cells for ASIBs.

2. Iron-Based Cathode Materials

Cathode materials generally play a decisive role in full cell energy density, and are expected to exhibit a high reaction potential and a high capacity. To date, Fe-based cathode materials primarily include polyanionic compounds (phosphates, pyrophosphates, and mixed anions) and Prussian blue analogues (PBA).

2.1. Polyanionic Compounds

Recently, polyanionic compounds have received extensive attention for ASIBs, due to their stable structures and tunable reaction potentials. In this paper, we will start with the $NaFePO_4$ material, which is one of the earliest compounds in ASIB research. This material also attracted considerable interest at the beginning of ASIB research. Then, we will discuss other polyanionic compounds that show better performance than the $NaFePO_4$ material.

2.1.1. $NaFePO_4$ Cathode

Phosphate compounds are promising electrode materials for battery applications, due to their versatile crystal structures, stable P-O bonds, and relatively high reaction potentials [63]. One of the most representative phosphate examples is the $LiFePO_4$ cathode, which was first developed by John Goodenough in 1997 and is now used as a leading cathode in some electric vehicles [64,65]. The $LiFePO_4$ material exhibits an olivine structure (space group: Pnma) and has a one-dimensional Li^+ diffusion channel, which leads to a two-phase transition reaction between $LiFePO_4$ and $FePO_4$ (Figure 3a). As a result, the $LiFePO_4$ features a flat reaction potential of +3.45 V vs. Li^+/Li, a high theoretical capacity of ~170 mAh g^{-1}, and superior cycling performance [64,65]. Due to these attractive properties of $LiFePO_4$, its sodium version, $NaFePO_4$, naturally receives immediate attention in early-stage ASIB studies.

However, the Li^+/Na^+ ion size difference is large in crystal structures, as are the differences in the reaction mechanisms in the $AFePO_4$ framework (A = Li and Na). Unlike olivine $LiFePO_4$, $NaFePO_4$ crystalizes in two distinct crystal structures, i.e., maricite and olivine [66]. The maricite phase is thermodynamically more stable, but it does not exhibit a well-defined Na^+ diffusion channel (Figure 3b) [67,68]. Consequently, the maricite phase is electrochemically inactive for Na^+ insertion, and research efforts have focused on the olivine $NaFePO_4$ phase. Based on the Fe^{2+}/Fe^{3+} redox couple, the olivine $NaFePO_4$ cathode exhibits a high theoretical capacity of 154 mAh g^{-1}.

To prepare olivine $NaFePO_4$, researchers generally use olivine $LiFePO_4$ as the starting compound, extract Li^+ ions from its structure, and then, re-insert Na^+ ions to form an olivine $NaFePO_4$ phase (Figure 3a). In 2013, Mentus et al. used the electrochemical ion-exchange method to prepare a $NaFePO_4$ material [69], where $LiFePO_4$ was subjected to successive cyclic voltammetry (CV) scanning in a saturated $NaNO_3$ electrolyte. Compared with $LiFePO_4$, $NaFePO_4$ exhibits a 0.3 V lower reaction potential (Figure 3c). Moreover, $NaFePO_4$ has one cathodic peak but demonstrates two anodic peaks, which are due to the intermediate phase of $Na_{2/3}FePO_4$ during the charging process. In this study, the authors used CV to explore electrochemical performance, but the galvanostatic charge/discharge (GCD) properties remain unknown.

In 2015, Cabanas et al. used a chemical method to prepare an olivine $NaFePO_4$ material and systematically compared its Na insertion performance in aqueous and non-aqueous electrolytes [70]. They first used nitronium tetrafluoroborate (NO_2BF_4) to oxidize $LiFePO_4$ into $FePO_4$, and then, they utilized sodium iodide (NaI) to reduce $FePO_4$ into $NaFePO_4$. They found that $NaFePO_4$ demonstrated much faster reaction kinetics and lower polarization in aqueous Na_2SO_4 electrolytes than non-aqueous $NaClO_4$/EC-PC (EC: ethylene carbonate; PC: propylene carbonate) electrolytes. At a rate of 0.1 C, the polarization was 0.27 V in aqueous electrolytes (Figure 3d), lower than 0.44 V in non-aqueous electrolytes. When tested in the same potential range, aqueous electrolytes led to good capacity utilization of 50% at a rate of 2 C (Figure 3d), whereas non-aqueous ones showed a minimal reaction capacity. These results indicate that $NaFePO_4$ could work as a higher-rate cathode in ASIBs. Then, the authors assembled an ASIB full cell of $NaFePO_4||NaTi_2(PO_4)_3$, which exhibited a cell voltage of ~0.6 V and stable cycling of 20 cycles. This work systematically investigated $NaFePO_4$ battery performance in aqueous electrolytes, but the overall performance appears premature, which warrants further improvement. For instance, the $NaFePO_4$ cathode only delivered a moderate capacity of ~75 mAh g^{-1} at room temperature, which corresponds to only 50% of the theoretical capacity. When the temperature increased to 55 °C, this cathode managed to give ~110 mAh g^{-1}. Meanwhile, the $NaFePO_4$ cycling performance was not satisfactory. The authors found that NaFePO4 suffered from fast capacity fading in a wider potential range of −0.2~0.6 V vs. SHE, and they excluded the material dissolution reason based on inductively coupled plasma (ICP) analysis. Thus, the capacity decay mechanism requires further investigation.

In 2019, Tron et al. investigated the capacity fading mechanism in $NaFePO_4$ and proposed an artificial aluminum fluoride (AlF_3) coating to enhance its cycling life [71]. They found that surface deterioration was primarily responsible for the poor cycling in bare $NaFePO_4$, where the electrode–electrolyte side reactions led to the formation of iron oxides or iron hydroxides. To address this issue, they coated AlF_3 on the $NaFePO_4$ surface for electrode protection. Consequently, the coated electrode not only exhibited a higher initial Coulombic efficiency, but also demonstrated better cycling stability (Figure 3e). Unfortunately, even with surface coating, the $NaFePO_4$ cathode was still limited to 50 cycles, which is much inferior to non-aqueous systems. For instance, Loh et al. reported that $NaFePO_4$ showed outstanding capacity retention of 70% after 6000 cycles in non-aqueous electrolytes [72]. Therefore, there is a large performance gap between non-aqueous and aqueous electrolytes, and sophisticated characterization methods are needed to understand the capacity fading mechanism, which will help to demonstrate a long-cycling $NaFePO_4$-based ASIB. For instance, electrochemical quartz crystal microbalance (EQCM) tests might provide alternative insights into the interfacial ion insertion process [73]. Pan et al. and Cakan et al. carried out in situ EQCM tests of the $NaFePO_4$ electrode in aqueous electrolytes, and the reaction mass ratios were found to be 31–33 g mol^{-1} and 36–39 g mol^{-1}, respectively [73,74]. Although these two studies have some discrepancies, it is evident that both Na^+ ions and water molecules participate in surface redox reactions, because the molar mass of naked Na^+ ions is 23 g mol^{-1}. The participation of water molecules may explain the formation of FeO or $Fe(OH)_2$ on the $NaFePO_4$ surface, which leads to the capacity fading.

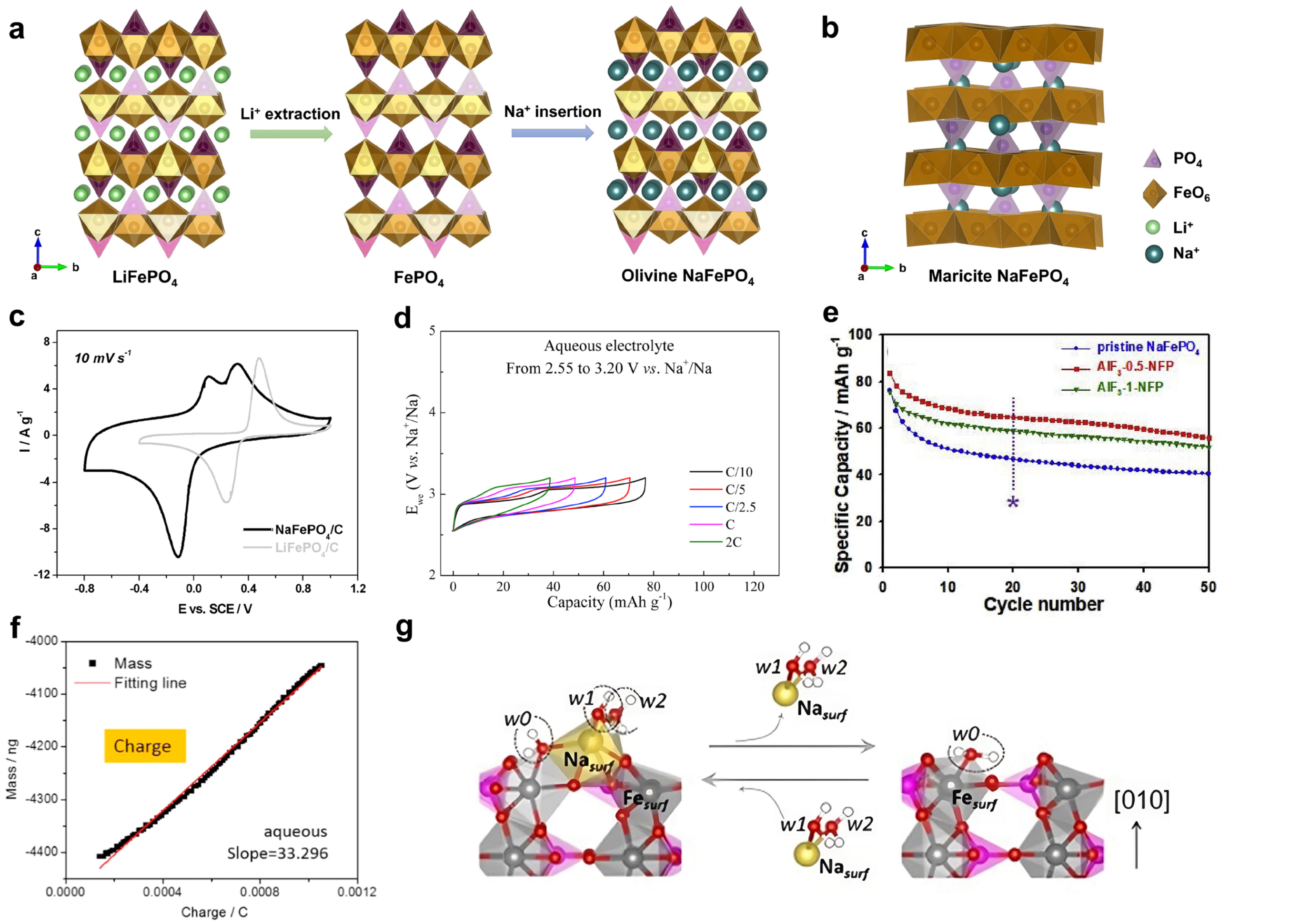

Figure 3. (**a**) The structural transition between olivine $LiFePO_4$, olivine $FePO_4$, and olivine $NaFePO_4$. (**b**) The crystal structure of maricite $NaFePO_4$. (**c**) A CV curve comparison between the Li insertion in $LiFePO_4$ and Na insertion in $NaFePO_4$. Reprinted from reference [70], with permission from Elsevier. (**d**) The rate performance of NaFePO4 in aqueous electrolytes. Reprinted from reference [70], with permission from Elsevier. (**e**) A cycling performance comparison between bare $NaFePO_4$ and AlF_3−coated $NaFePO_4$. The * in the Figure 3e indicates the cycling performance comparison at 20th cycle. Reprinted from reference [71], with permission from Elsevier. (**f**) EQCM analysis of the Na insertion process in $NaFePO_4$. Reprinted from reference [73], with permission from Elsevier. (**g**) Theoretical simulations on Na insertion in $NaFePO_4$ in aqueous electrolytes. Reprinted from reference [73], with permission from Elsevier.

Another drawback related to the olivine $NaFePO_4$ cathode is the complicated synthesis route, where $LiFePO_4$ needs to serve as a sacrificial template, and it undergoes a two-step synthetic oxidation–reduction route. To solve this issue, Manjunatha et al. reported a low-temperature ionothermal method to prepare an olivine $NaFePO_4$ material [75], where the reaction medium was a deep eutectic solvent, and the temperature was as low as 200 °C. When paired with a $NaTi_2(PO_4)_3$ anode in 5 M $NaNO_3$ electrolytes, the $NaFePO_4$ cathode delivered a good capacity of ~97 mAh g^{-1} at a rate of 0.2 and reasonable capacity retention (78%) over 50 cycles.

2.1.2. Other Polyanionic Compounds

Besides the intensive studies on the $NaFePO_4$ cathode, other Fe-based phosphate materials have also attracted certain attention for ASIBs. However, due to the limited number of publications, we will discuss these materials in one section and categorize them as other polyanionic compounds.

Compared with $NaFePO_4$, sodium iron pyrophosphate ($Na_2FeP_2O_7$) exhibits a relatively higher Na insertion potential, due to the stronger inductive effect of the $[P_2O_7]^{4-}$ groups [76,77]. More importantly, $Na_2FeP_2O_7$ could be readily synthesized via a conventional solid-state method [76,77], which does not need to use lithium compounds as the starting precursor. This is beneficial for large-scale synthesis. $Na_2FeP_2O_7$ has a triclinic crystal structure (P-1, No.2) and exhibits a theoretical capacity of ~97 mAh g^{-1} based on one-electron Fe^{2+}/Fe^{3+} redox, which is lower than $NaFePO_4$ but still acceptable as a Na-ion cathode.

Kim et al. used a simple solid-state method and prepared a carbon-coated $Na_2FeP_2O_7$ material [78]. They found that aqueous electrolytes led to lower polarization and faster rate performance than non-aqueous electrolytes, which is akin to the $NaFePO_4$ case. The $Na_2FeP_2O_7$ electrode delivered a good capacity of ~87 mAh g^{-1} in a wide potential range of −0.26~0.94 V vs. SHE, with an average potential of ~0.25 V vs. SHE (Figure 4a). However, the capacity decreased to ~65 mAh g^{-1} in a narrow range of 0.04~0.94 V. This cathode showed an impressive rate performance of 50 C and excellent capacity retention of 86% after 300 cycles. Apparently, the $Na_2FeP_2O_7$ cathode exhibited better cycling stability than $NaFePO_4$. The authors also used advanced characterization tools to investigate the reaction mechanism. Fe-edge X-ray absorption near edge structure (XANES) analysis revealed that Fe element valance changes from +2 to +3 during the charge process, which indicates the oxidization of $Na_2FeP_2O_7$. They also performed ex situ XRD analysis of the cycled electrode, which showed no peak change or intensity degradation, confirming the reaction reversibility. Later, Okada et al. further investigated electrolytes' influence on $Na_2FeP_2O_7$ performance, [79] where three different electrolytes were compared, i.e., Na_2SO_4 (2.0 M), $NaNO_3$ (4.0 M), and $NaClO_4$ (4.0 M). They found that these electrolytes led to similar cycling for $Na_2FeP_2O_7$, but $NaNO_3$ showed the worst cycling for the $Na_2FeP_2O_7||NaTi_2(PO_4)_3$ full cell, due to the nitrate decomposition and electrode corrosion reactions. Considering the strong oxidizing capabilities and potential explosiveness of sodium perchlorate, the authors concluded that 2.0 M Na_2SO_4 is the most promising electrolyte for aqueous $Na_2FeP_2O_7||NaTi_2(PO_4)_3$ full cells, which maintain ~89% capacity over 30 cycles.

Despite the easy synthesis of $Na_2FeP_2O_7$, its moderate potential and relatively low capacity restrict the energy density of ASIB full cells. Hence, it is crucial to develop other Fe-based materials with higher potentials or capacities. $Na_4Fe_3(PO_4)_2P_2O_7$ is an interesting mixed polyanionic material, [80] which adopts an orthorhombic structure (space group: $Pn2_1a$) with large open channels. This material exhibits an even higher potential than $NaFePO_4$ and $Na_2FeP_2O_7$. The Fe ions exist in their 2+ state, and theoretically, all these Fe^{2+} ions could be oxidized to Fe^{3+}. Consequently, this material can support the 3-Na insertion reaction, which corresponds to a theoretical capacity of ~129 mAh g^{-1}. Compared with $Na_2FeP_2O_7$, $Na_4Fe_3(PO_4)_2P_2O_7$ shows both a higher capacity and a higher reaction potential. Cabanas et al. studied $Na_4Fe_3(PO_4)_2P_2O_7$ performance in 1 M Na_2SO_4 electrolytes, [81] which delivered a specific capacity of ~84 mAh g^{-1} and an average potential of ~0.30 V vs. SHE (Figure 4b). However, the cycling stability of $Na_4Fe_3(PO_4)_2P_2O_7$ is less satisfactory, with 74% capacity retention in 50 cycles. To understand the capacity fading mechanism, the authors of [81] immersed $Na_4Fe_3(PO_4)_2P_2O_7$ in electrolytes and used ICP to detect the dissolved iron and phosphorus concentration, which were found to be 0.1% and 2.1%, respectively. Due to the much higher phosphorus content, it is likely that pyrophosphate anions undergo hydrolysis side reactions, which result in active mass loss and iron oxide precipitation. Therefore, surface coating could be necessary to reinforce cycling stability.

Na_2FePO_4F represents another promising ASIB cathode with a high reaction potential, due to the presence of electron-withdrawing fluoride anions [82]. Meanwhile, this cathode exhibits a theoretical capacity of 124 mAh g^{-1}, comparable to $Na_4Fe_3(PO_4)_2P_2O_7$. This material crystalizes in an orthorhombic crystal structure with a space group of Pbcn.

Barpanda et al. first studied Na_2FePO_4F performance in a concentrated electrolyte of 17 m $NaClO_4$ (m: mol kg^{-1}) [83], which may help to inhibit the material dissolution. As a result, Na_2FePO_4F delivers a capacity of ~84 mAh g^{-1} (Figure 4c), a high-rate capability of 5.0 mA cm^{-2}, and stable cycling of 100 cycles. When coupled with a $NaTi_2(PO_4)_3$ anode, the full cell shows a moderate cell voltage of ~0.7 V and decent cycling retention of 65% over 100 cycles. Relatively inferior cycling in full cells should result from the capacity fading on the anode side.

Besides $[P_2O_7]^{4-}$ and F^- anions, carbonate anions have also been introduced to the Na-Fe-PO system to make new compounds. For instance, $Na_3FePO_4CO_3$ is another promising cathode with a theoretical capacity of ~191 mAh g^{-1}, due to its potential two-Na insertion via Fe^{3+}/Fe^{2+} and Fe^{3+}/Fe^{4+} redox couples. [84] This capacity even exceeds the $NaFePO_4$ material. In 2020, Okada et al. briefly reported its Na insertion performance in a conference abstract, [79] which described an initial charge/discharge capacity of ~130/112 mAh g^{-1} in 17 m $NaClO_4$ electrolytes. However, other information, such as electrochemical or structural characterization, is not available. In 2021, Manjunatha et al. systematically investigated $Na_3FePO_4CO_3$'s battery performance in a 2.0 M Na_2SO_4 electrolyte [85]. In a typical CV test, the $Na_3FePO_4CO_3$ electrode demonstrated a pair of oxidization/reduction peaks at 0.54/0.32 V vs. SCE (SCE: saturated calomel electrode), which converted to 0.78/0.56 V vs. SHE. On average, the Na insertion potential was 0.67 V vs. SHE, which is much higher than that of previous Fe-based materials. However, the potential gap of 0.22 V was not negligible, which indicates sluggish Na insertion kinetics. As a result, the GCD tests revealed that this cathode delivers a moderate capacity of ~80 mAh g^{-1} and considerable polarization of 0.5 V (Figure 4d), which leads to very low energy efficiency. When paired with the common $NaTi_2(PO_4)_3$ anode, the full cell exhibited a reasonable rate capability of 2C and stable cycling of 100 cycles. Nevertheless, GCD curves were not shown for full cells, and the voltage hysteresis, energy density, and power density remain unknown.

2.2. Prussian Blue Analogues

In addition to polyanionic compounds, Prussian blue analogues (PBAs) represent another class of Fe-based materials for ASIBs. PBAs exhibit a general chemical formula of $A_xM[Fe(CN)_6]_y\cdot\square_{1-y}\cdot zH_2O$ ($0 \leq x \leq 2$, $0 \leq y \leq 1$; z varies with the experimental conditions), where A, M, and $\square$ stand for alkali metals, transition metals, and $Fe(CN)_6$ vacancies, respectively [86]. PBAs usually possess a face-centered cubic structure, which is built up via the three-dimensional connection of Fe-CN-M bonds. The alkali metal cations and zeolitic water molecules occupy the center of nano-voids. Compared with iron-based polyanionic materials, PBAs hold greater promise for ASIBs. Firstly, PBAs theoretically undergo a 2-Na insertion reaction, which leads to a high theoretical capacity of ~170 mAh g^{-1} [87]. Secondly, the $[Fe(CN)_6]^{3-}/[Fe(CN)_6]^{4-}$ redox couple exhibits a high reaction potential of +0.4~1.0 V vs. SHE, which is promising for cathode reactions [88]. Thirdly, the large open framework facilitates fast and reversible Na insertion reactions, which results in excellent rate and cycling performance [89]. Lastly, the synthesis of PBAs is based on an aqueous precipitation method [90], which is more cost-effective than the solid-state synthesis of iron phosphates. To date, there are several excellent review papers on PBA materials for non-aqueous and aqueous SIBs [20,91–93], and readers may refer to these publications for more information. Here, we limit our discussion to $Na_xFe[Fe(CN)_6]_y\cdot\square_{1-y}\cdot zH_2O$ materials only, considering that the focus is on the use of Fe-based materials for ASIBs.

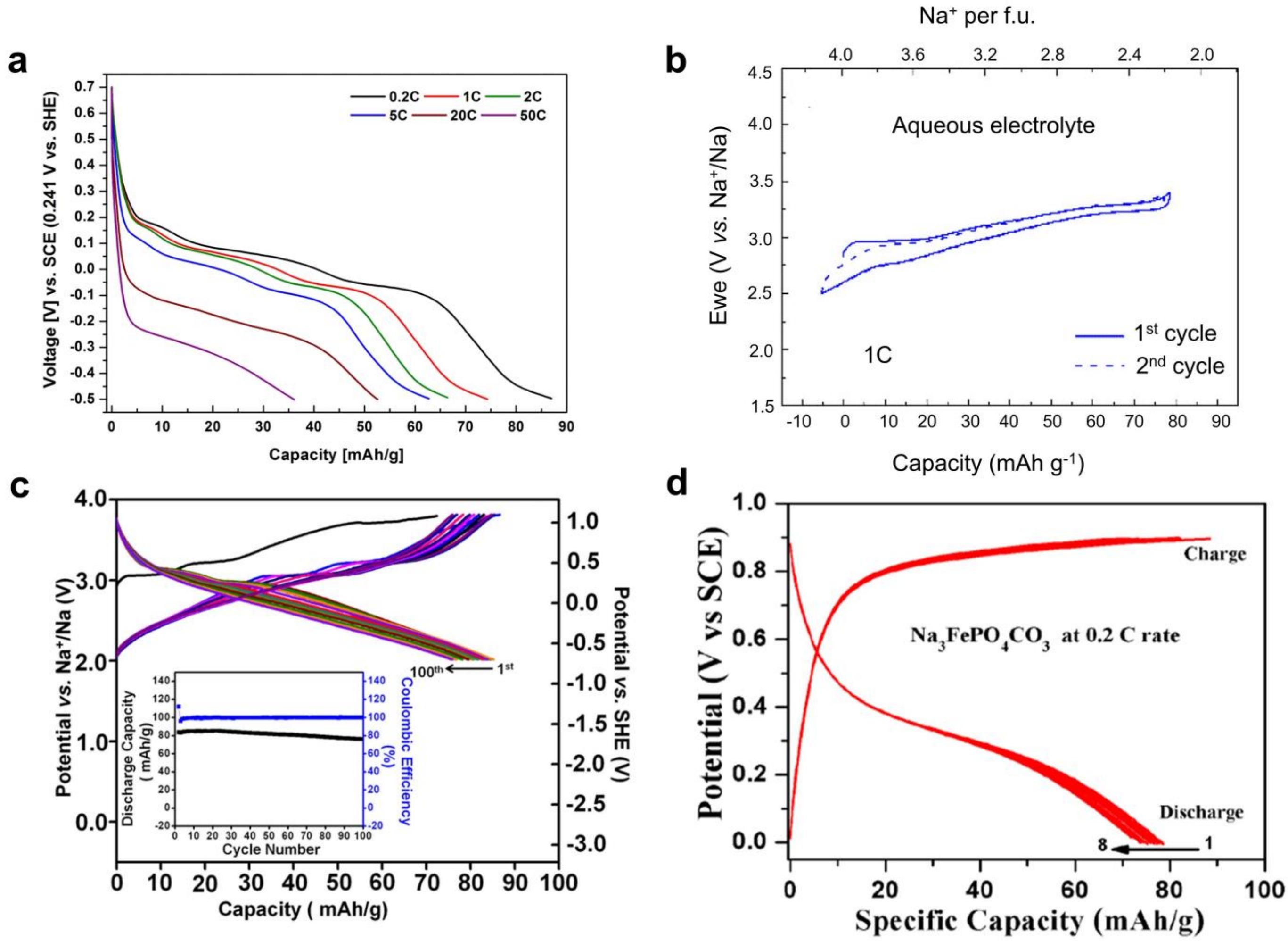

Figure 4. Electrochemical performance of other Fe−based polyanionic compounds. (**a**) The discharge curves of the $Na_2FeP_2O_7$ cathode. Reprinted from reference [78], with permission from authors. (**b**) GCD curves of the $Na_4Fe_3(PO4)_2P_2O_7$ cathode. Reprinted with permission from reference [81]. Copyright 2018 American Chemical Society. (**c**) GCD curves of the Na_2FePO_4F cathode, where the inset is the cycling performance. Reprinted with permission from reference [84]. Copyright 2018 WILEY−VCH Verlag GmbH & Co. KGaA. (**d**) GCD curves of the $Na_3FePO_4CO_3$ cathode. Reprinted from reference [85], with permission from IOP Publishing.

Based on the valence state of carbon-coordinated and nitrogen-coordinated iron ions, the $Na_xFe[Fe(CN)_6]_y\cdot\square_{1\text{-}y}\cdot zH_2O$ material can be further divided into Prussian yellow (PY, +3 and +3), Prussian blue (PB, +2 and +3), and Prussian white (PW, +2 and +2) [88], as shown in Figure 5a. Note that in the PB structure, the carbon-coordinated and nitrogen-coordinated iron are in a +2 and +3 state, respectively. It is known that $Fe(CN)_6$ vacancies degrade PBA crystal structures and lead to low capacities and capacity fading [89,90,94–96]. To suppress these vacancies, Yang et al. used a slow crystallization method and prepared a low-defect PY compound of $Fe[Fe(CN)_6]_{0.87}\cdot\square_{0.13}$ [21], that contained only 13% $Fe(CN)_6$ vacancies, much lower than the 25–30% in conventional PBAs. When tested for ASIBs, this PY cathode delivered a high capacity of ~125 mAh g^{-1} (Figure 5b) and stable cycling of 500 cycles with 83% retention. It also showed an encouraging rate performance of 20 C, which surpasses most iron phosphate materials. By contrast, the conventional PBA materials with 30% $Fe(CN)_6$ vacancies suffered from severe capacity fading (Figure 5c). Li et al. further compared Li insertion and Na insertion in PY structures [97]. Interestingly, PY supported a reversible Na insertion reaction with a good capacity of ~120 mAh g^{-1}, but it exhibited fast capacity fading for Li-ion insertion. The inferior Li-ion cycling was due to the very large size of hydrated Li^+ ions, which cannot easily enter PBA channels. By contrast, Na^+ ions can become de-solvated and readily enter PBA structures. This comparison further highlights the promise of PBAs for ASIB applications.

Regardless of the high capacity and stable cycling of PY materials, they do not have removable Na+ ions in their initial structures, which challenges full cell assembly. Yang et al. attempted to use sodium iodide (NaI) to reduce the PY compound, but the amount of introduced Na^+ ions was quite limited [21]. Therefore, it is more favorable to directly prepare Na-rich PBA materials. In 2016, Cabanas et al. prepared a PB material of $Na_{0.75}Fe_{1.08}[Fe(CN)_6]\cdot 3.5H_2O$ and studied its performance in 1 M Na_2SO_4 electrolytes [98]. When tested in a controlled voltage range, this cathode delivered a moderate capacity of ~61 mAh g^{-1} (Figure 5d) and stable cycling of 200 cycles with 84% retention. To further enhance the cycling performance, Huang et al. prepared a similar PB material of $Na_{0.65}Fe[Fe(CN)6]_{0.91}\cdot\square_{0.09}\cdot 2.7H_2O$ and developed a graphene oxide (GO) suspension-based electrolyte [99]. GO's introduction to 1 m $NaClO_4$ electrolyte formed an ion-selective membrane on the separator, which helped to suppress the Fe^{3+} dissolution and crossover to the anode. Therefore, this new electrolyte led to superior long cycling of 17,000 cycles with 65.1% capacity retention, which would be the longest cycling among all the Fe-based ASIB materials. However, we need to note that the moderate Na^+ concentration (0.65) in the structure will inevitably lead to a low initial charge capacity, which still complicates the full cell assembly.

In comparison with PY and PB, the PW material $Na_2FeFe(CN)_6$ is the most promising choice for full cell applications. However, this material is prone to oxidization because both Fe ions exist in the +2 state, so it requires delicate material synthesis and protection. Wu et al. used $Na_4Fe(CN)_6$ as the single iron source and added sodium chloride, hydrogen chloride, and poly-(vinylpyrrolidone) to synthesize the PW material [100]. Well-defined PW cubes (~2 μm) were obtained, and the chemical formula was found to be $Na_{1.29}Fe[Fe(CN)_6]_{0.91}\cdot\square_{0.09}$, which exhibited higher Na content than previous PB materials. This cathode showed a good capacity of ~107 mAh g^{-1} and minimal capacity fading after 1100 cycles. When paired with an activated carbon for a hybrid capacitor, the device exhibited an average voltage of ~0.8 V and energy density of ~30 Wh kg^{-1}. Later, Zhang et al. used a citrate-assisted co-precipitation method to prepare PW compounds [101], where ascorbic acid was added to prevent Fe^{2+} oxidation. As a result, they achieved an even higher Na content and obtained a chemical formula of $Na_{1.74}Fe[Fe(CN)_6]_{0.94}\cdot\square_{0.06}\cdot 3.3H_2O$. This PW material exhibited a high capacity of ~120 mAh g^{-1} (Figure 4e) and a high rate capability of 3000 mA g^{-1}. However, the cycling stability was not satisfactory, with 32% capacity retention over 1000 cycles. The authors thus doped 24% nickel ions into the PW structure, which stabilized the crystal structure and led to 73% capacity retention over 1000 cycles (Figure 5f).

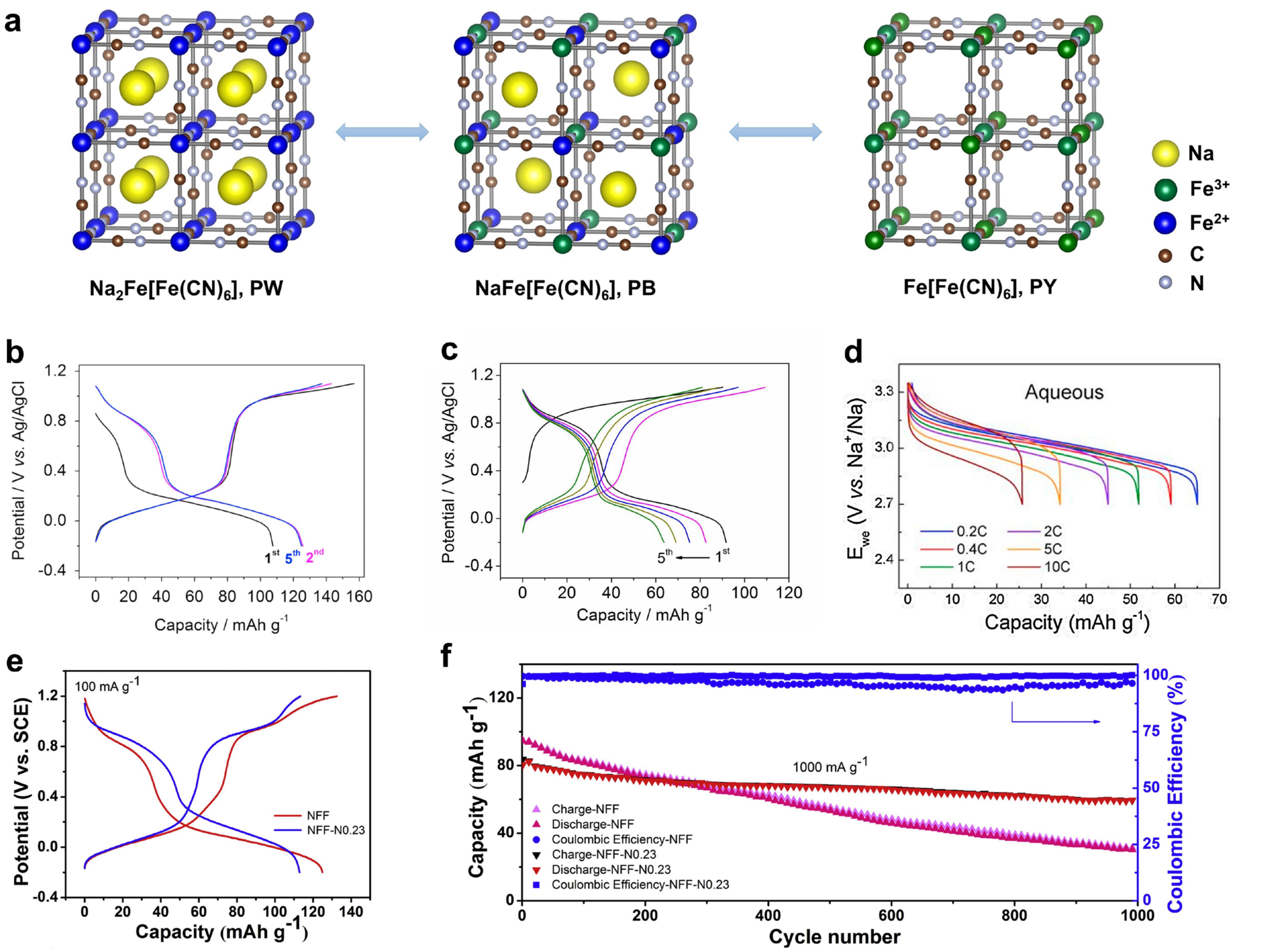

Figure 5. Structural and electrochemical properties of PBA materials. (**a**) The structural transition between $FeFe(CN)_6$, $NaFeFe(CN)_6$, and $Na_2FeFe(CN)_6$ materials. (**b**) GCD curves of the low−vacancy $FeFe(CN)_6$ material. Reprinted from reference [21], with permission from Elsevier. (**c**) GCD curves of the conventional $NaFeFe(CN)_6$ material with high vacancies. Reprinted from reference [21], with permission from Elsevier. (**d**) GCD curves of the $NaFeFe(CN)_6$ cathode. Reprinted from reference [98], with permission from Elsevier. (**e**) GCD curves of the $Na_2FeFe(CN)_6$ and nickel−doped $Na_2FeFe(CN)_6$ materials. Reprinted from reference [101], with permission from Elsevier. (**f**) A cycling performance comparison between pure $Na_2FeFe(CN)_6$ and nickel−doped $Na_2FeFe(CN)_6$ cathode. Reprinted from reference [101], with permission from Elsevier.

3. Iron-Based Anode Materials

To date, most ASIBs have utilized $NaTi_2(PO_4)_3$ as the prominent anode material [102], due to its good capacity of 100–120 mAh g^{-1} and low reaction potential of −0.6 V vs. SHE. However, titanium-based materials are generally expensive, which increases the overall cost of ASIBs. Moreover, the Ti^{4+}/Ti^{3+} redox potential is low enough to trigger noticeable HER side-reactions (−0.4 V vs. SHE) in conventional aqueous electrolytes [102]. In this regard, Fe-based anode materials represent an attractive direction, because of their much lower cost and slightly higher redox potentials. Currently, Fe-based anode materials include iron phosphates, oxides, carbides, and selenides.

3.1. Phosphate Materials

Iron phosphate materials are generally used as cathode materials in non-aqueous SIBs, and their average insertion potentials range from 2.3 to 3.0 V vs. Na^+/Na [103]. If converted to aqueous electrolytes, these potentials are −0.4~0.3 V vs. SHE, suggesting that some phosphates can serve as anode candidates for aqueous SIBs.

In 2018, Zaghib et al. reported an amorphous iron phosphate hydrate ($FePO_4 \cdot 2H_2O$) as a low-cost and cycle-stable anode for ASIBs [104]. This material is commercially available with a low price of ~300 USD/ton, which is much lower than $NaTi_2(PO4)_3$ (~10,000 USD/ton). Based on Fe^{3+}/Fe^{2+} redox, this material can host 1 Na^+ per formula and transforms to $NaFePO_4$, corresponding to a high theoretical capacity of ~143 mAh g^{-1}. Figure 6a shows the proposed Na^+ diffusion pathway in its structure. When tested in 1 M Na_2SO_4, this anode delivered a moderate capacity of ~70 mAh g^{-1} (Figure 6b), which represents only 50% capacity utilization. The average insertion potential was ~0 V vs. SHE, which is much higher than $NaTi_2(PO_4)_3$, and thus, effectively avoids HER reactions. However, the high potential in the anode led to low voltage in the full cell system. When paired with a $Na_{0.44}MnO_2$ cathode, the full cell only showed a low voltage of ~0.5 V, which is not suitable for practical use. Moreover, the half-cell and full-cell cycling performances were limited to 200 (Figure 6c) and 300 cycles, respectively.

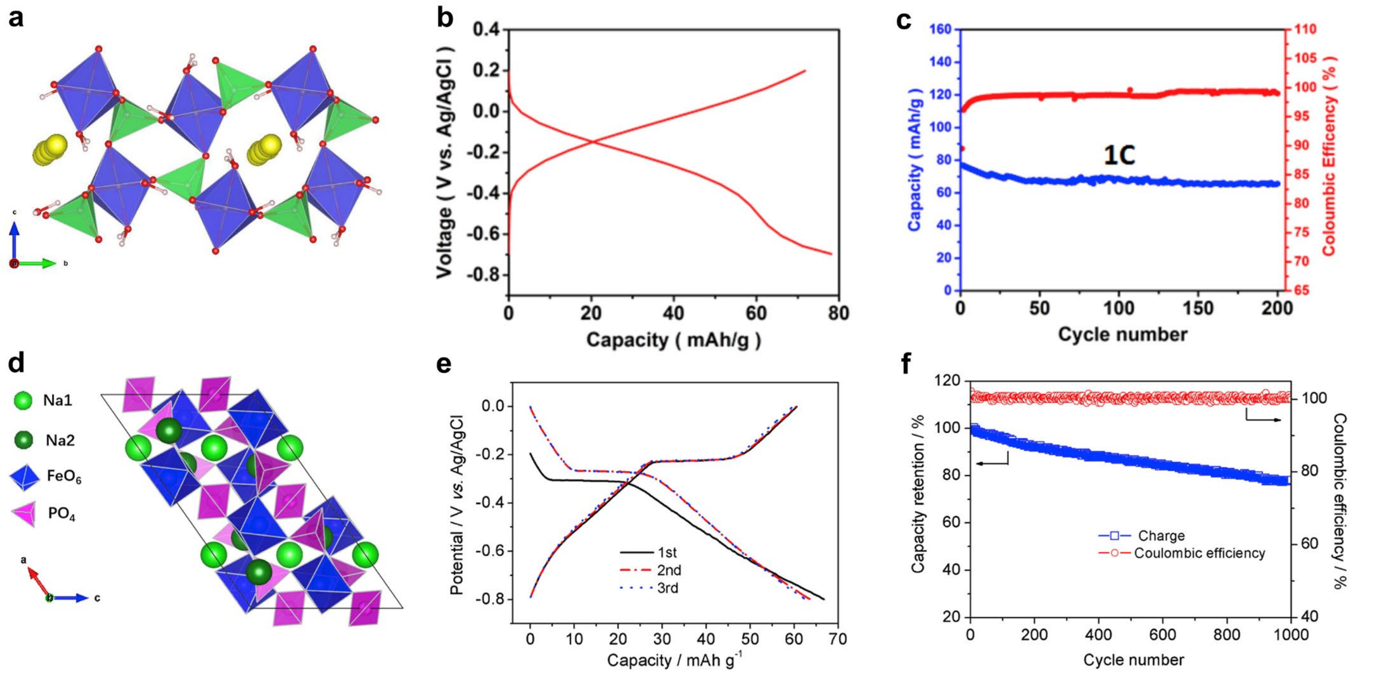

Figure 6. Structural and electrochemical properties of iron phosphate anode materials. (**a**) The crystal structure and Na–diffusion manner in the hydrated $FePO_4 \cdot 2H_2O$ material. The yellow circles represent the Na+ ions. The green tetrahedron is the [PO_4] group, while the blue octahedron is the [FeO_6] group. (**b**) GCD curves of the $FePO_4 \cdot 2H_2O$ anode. (**c**) The cycling performance of the $FePO_4 \cdot 2H_2O$ anode. (**a**–**c**) were reprinted from reference [103], with permission from Elsevier. (**d**) Crystal structures of the NASICON $Na_3Fe_2(PO_4)_3$. (**e**) GCD curves of the $Na_3Fe_2(PO_4)_3$ anode. (**f**) Cycling performance of the $Na_3Fe_2(PO_4)_3$ anode. (**d**–**f**) were reprinted from reference [104,105], with permission from Elsevier.

To further improve anode performance, Feng et al. investigated other iron phosphate materials with different stoichiometries and crystal structures [105,106]. In 2019, they presented a NASICON-type $Na_3Fe_2(PO_4)_3$ (Figure 6d) as a low-cost, high-rate, and long-cycling anode material in 17 m $NaClO_4$ electrolytes. [105] By utilizing the Fe^{3+}/Fe^{2+} redox couple, this anode could host 1 Na^+ and exhibited a reasonable capacity of ~60 mAh g^{-1} (Figure 6e). Its reaction potential of ~0 V vs. SHE is close to the previously reported value for $FePO_4 \cdot 2H_2O$, but it exhibited a much better rate capability of 100 C and excellent cycling of 1000 cycles (Figure 6f), which likely resulted from the stable NASICON crystal structures and well-defined Na insertion channels. Ex situ XRD analysis revealed the formation of a $Na_4Fe_2(PO_4)_3$ phase at the end of discharge, which accounts for the reaction plateau at

~0 V. Additionally, X-ray photoelectron spectroscopy (XPS) showed that the Na/Fe ratio increased from 1.55 to 1.94 when the electrode was fully discharged, which further confirms the formation of $Na_4Fe_2(PO_4)_3$.

In 2021, Feng et al. demonstrated another layer-structured $Na_3Fe_3(PO_4)_4$ material as a high-performance anode [106]. This material accommodates two Na^+ ions, and thus, exhibited a higher capacity of ~80 mAh g^{-1}, which surpasses $FePO_4{\cdot}2H_2O$ and $Na_3Fe_2(PO_4)_3$. Additionally, the reaction potential was found to be −0.2 V vs. SHE, lower than $NaTi_2(PO_4)_3$ (−0.6 V) but higher than HER (−0.4 V), which enabled the maintenance of a good balance between full cell voltages and water decomposition reactions. Furthermore, its desirable layered structure with roomy spaces facilitated a fast and reversible Na insertion process, which translated to a predominantly high rate of 200 C and extremely long cycling of 6000 cycles with 72% retention. Such electrode performance has set a record in Fe-based anode materials. The authors used in operando synchrotron XRD and Fe K-edge XANES spectra to study the reaction mechanism. During the discharge, there was no extra XRD peak, and the (200), (110), and (022) peaks progressively shifted to lower positions. This means that the $Na_3Fe_2(PO_4)_3$ anode works on a solid-solution Na insertion reaction, where the lattice structure expands when the Na^+ insertion takes place. The binding energy of the Fe element also moved to a lower energy value, which indicates an Fe^{3+}/Fe^{2+} redox reaction. On average, the Fe valance state lowered from +3 to +2.3, which corresponds to a two-Na insertion reaction. Therefore, the Na insertion reaction is a reversible transition between the $Na_3Fe_3(PO_4)_4$ and $Na_5Fe_3(PO_4)_4$ materials.

3.2. Oxides, Carbides, and Selenides

Iron oxides (Fe_2O_3 or Fe_3O_4) are highly abundant and cheap materials, and also receive some attention for ASIB anode applications. Lokhande et al. deposited Fe_2O_3 thin film on stainless steel and evaluated its performance in 1 M Na_2SO_4, which showed a capacity of 78.6 mAh g^{-1} at 5 mV s^{-1} in a voltage range of 1.0 V [107]. This capacity is reasonable, but thin films have low mass loading and are not suitable for practical applications. Nwanya et al. synthesized nano-sized α-Fe_2O_3 spheres and tested their performance in 0.5 M Na_2SO_4 [108]. When scanned in a wide electrochemical window of −0.8 to 1.0 V vs. Ag/AgCl, this material delivered a very low capacity of 65 C g^{-1}, which corresponds to ~18 mAh g^{-1} only. The low capacity could have resulted from the capacitive reaction mechanism and higher mass loading. To pursue a higher capacity, Cheng et al. lowered the discharge cut-off potential to −1.4 vs. Ag/AgCl, which forced Fe_2O_3 to partially undergo conversion reactions [109]. As a result, it showed an enhanced capacity of ~80 mAh g^{-1} in 0.5 M Na_2SO_4 (Figure 7a). However, due to Fe ion dissolution, the capacity quickly faded to 0 mAh g^{-1} within 10 cycles (Figure 7b). Based on these results, it appears that Fe_2O_3 cannot maintain a high capacity and long cycling at the same time. Hence, researchers studied Fe_3O_4 as an alternative material. Ma et al. prepared an Fe_3O_4@rGO composite (rGO: reduced graphene oxide) and examined its Na insertion properties in 0.5 M Na_2SO_4 [110]. At 1 mA cm^{-2}, this anode exhibited a moderate capacity of ~64 mAh g^{-1} in a 1.0 V potential range. At 8 mA cm^{-2}, it also retained ~90% capacity over 1000 cycles, indicating a reversible Na^+ (de)absorption process.

Iron carbides (Fe_3C) are interesting materials due to their good chemical stability and thermal stability [111]. However, pure Fe_3C nanoparticles exhibit low electronic conductivity, which constrains their electrochemical performance. Wang et al. prepared porous Fe3C@rGO composites and tested their performance in 6 M KOH [112], where they demonstrated a capacity of ~95.3 mAh g^{-1}. They also assembled a full cell based on this anode and a $Na_{0.5}MnO_2$ cathode in 1 M Na_2SO_4, which supported a high charging voltage of ~2.4 V. However, the pure Na-storage performance of this anode was not shown. Moreover, the reaction mechanism remains elusive.

Iron selenides ($FeSe_2$) are another type of material that exhibits a high capacity in non-aqueous SIBs. However, they suffer from the material dissolution issue in aqueous electrolytes, due to the solubility og Se-based species [113]. To overcome this shortcoming, Xing et al. used GO to encapsulate $FeSe_2$ to form a composite electrode, which exhibited a moderate capacity of ~60 mAh g^{-1} and an average reaction potential of −0.35 V vs. SHE (Figure 6c) [113]. Compared with the pristine $FeSe_2$ electrode, the rGO coated one exhibited improved cycling performance over 100 cycles (Figure 7d). Ex situ XRD results revealed that the reaction mechanism is based on the conversion between $FeSe_2$ and $Na_xFe_2Se_4/Na_2Se$. The authors further assembled an $FeSe_2$@rGO-$Na_3V_2(PO_4)_2F_3$ full battery, which showed a high voltage (~1.7 V), good energy density (53.4 W h kg^{-1}), and excellent rate performance. However, the cycling performance was limited to 50 cycles only.

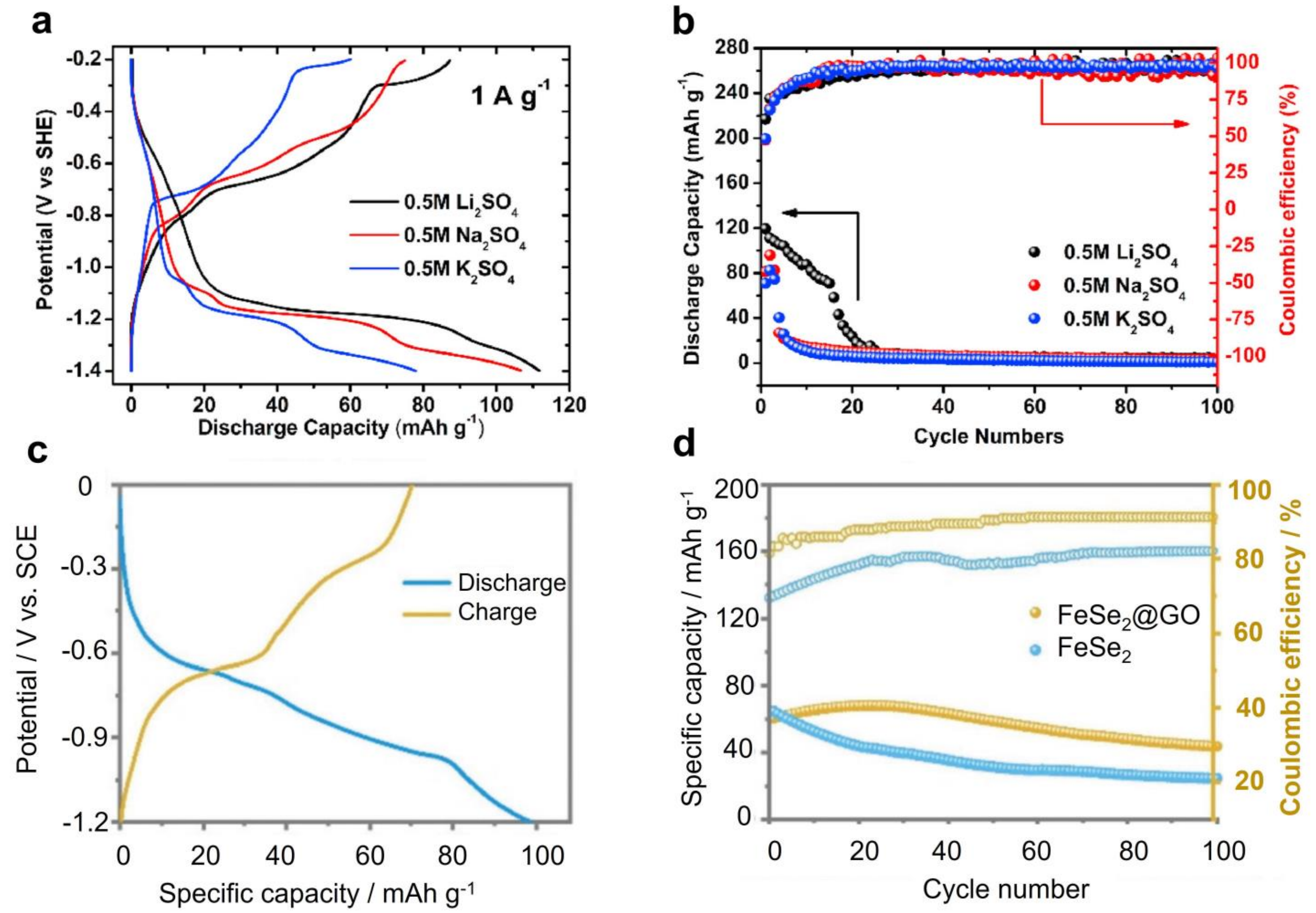

Figure 7. Electrochemical performance of Fe_2O_3 and $FeSe_2$. (**a**) GCD curves of the Fe_2O_3 anode for different cation storage. (**b**) The cycling performance of the Fe_2O_3 anode. Figure 6a,b were reprinted from reference [109], with permission from Elsevier. (**c**) GCD curves of the $FeSe_2$ anode. (**d**) A cycling performance comparison between pure $FeSe_2$ and $FeSe_2$@GO. Figure 6c,d were reprinted from ref−erence [113], with permission from the Royal Society of Chemistry.

4. Iron-Based ASIB Full Cells

Although many iron-based cathode and anode materials have been developed for half-cell studies, ASIB full cells, assembled from all-Fe-based materials, are under-explored. To our knowledge, there is only one full cell system that solely utilizes an Fe-based cathode and anode. In 2017, Yang et al. prepared an $Fe[Fe(CN)_6]$ (PY) material and used it in bipolar electrodes in ASIB full cells [114]. As discussed in the PBA section, two pairs of redox center exist in this material, which are nitrogen-coordinated and carbon-coordinated Fe^{3+}/Fe^{2+} couples, respectively. Their reaction potentials differ by ~0.70 V, which is reasonable for full cell operation. The authors pre-activated the PY electrode in a 1 M $NaNO_3$ electrolyte to prepare a Na-containing $NaFeFe(CN)_6$ material, which was used for full cell assembly (Figure 8a). The full cell reaction mechanism is expressed as follows:

$$NaFe^{III}[Fe^{II}(CN)_6] + NaFe^{III}[Fe^{II}(CN)_6] \leftrightarrow Fe^{III}[Fe^{III}(CN)_6] + Na_2Fe^{II}[Fe^{II}(CN)_6]$$

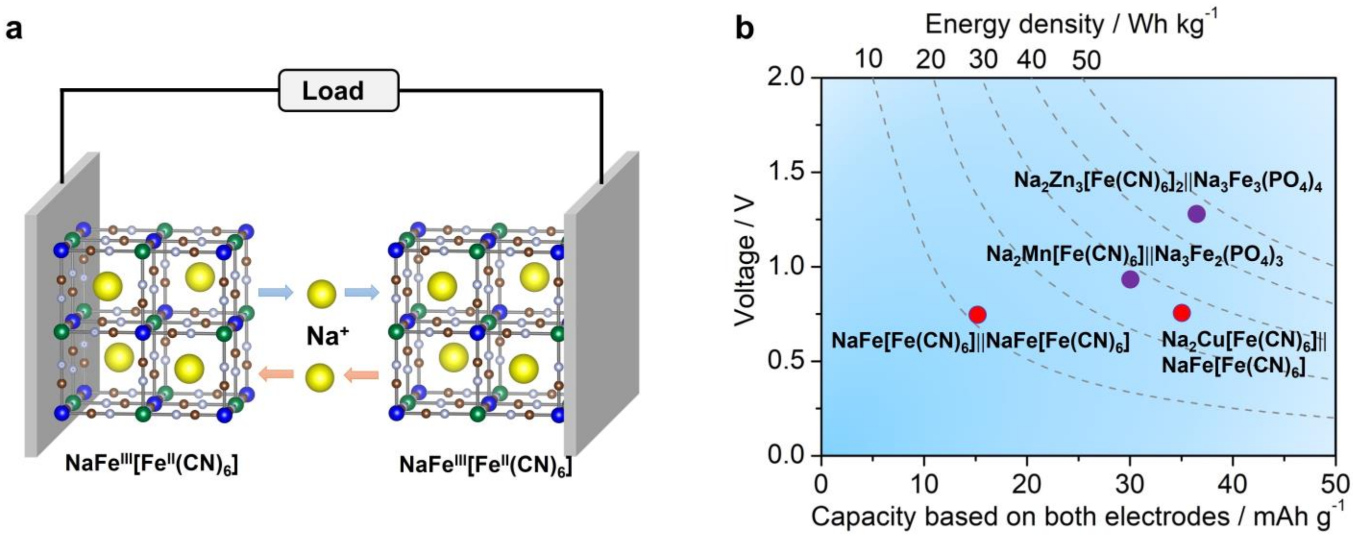

Figure 8. (**a**) A scheme of the all−PBA full cell system, where the cathode and anode are composed of the same $NaFe[Fe(CN)_6]$ material; (**b**) a capacity, voltage, and energy density comparison of different Fe−based ASIB full cells. The above figures were plotted by the authors.

This full cell delivered an average voltage of ~0.7 V, a high rate performance of 20 C, and stable cycling for 200 cycles. However, we need to point out that the average capacity was only ~14 mAh g^{-1} based on the total mass of the cathode and anode, which gave rise to low energy density of ~10 Wh kg^{-1}. This energy is too low to be practical.

Aside from Yang's work, there are several studies that incorporate other transition metals to increase the cell voltage and energy density of full cells, where the majority of the capacity still comes from Fe^{3+}/Fe^{2+} redox. For discussion purposes, we also include these works here. In 2019, Wang et al. used two PBA electrodes to fabricate an all-PBA-based ASIB [115]. The cathode was $Na_2Cu[Fe(CN)_6]$, while the anode was $NaFe[Fe(CN)_6]$. The full cell reaction is written as follows:

$$Na_2Cu[Fe^{II}(CN)_6] + NaFe^{III}[Fe^{II}(CN)_6] \leftrightarrow NaCu[Fe^{III}(CN)_6] + Na_2Fe^{II}[Fe^{II}(CN)_6]$$

Compared with $FeFe(CN)_6$ full cells, this ASIB system exhibited a similar cell voltage of ~0.70 V but higher energy density of ~27 Wh kg^{-1} (Figure 8b). It also delivered a good rate capability of 20 C and stable cycling of 250 cycles.

Feng et al. used another approach to develop Fe-based ASIB full cells, where the cathode was a PBA material, but the anode was an iron phosphate material [105,106]. In 2019, they assembled a full cell based on a $Na_2MnFe(CN)_6$ cathode, a $Na_3Fe_2(PO_4)_3$ anode, and concentrated electrolytes [99]. The full cell reaction can be written as follows:

$$Na_2Mn[Fe^{II}(CN)_6] + Na_3Fe^{III}{}_2(PO_4)_3 \leftrightarrow NaMn[Fe^{III}(CN)_6] + Na_4Fe^{III}Fe^{II}(PO_4)_3.$$

This full cell demonstrated an average cell voltage of ~0.9 V and energy density of ~27 Wh kg^{-1} (Figure 8b). It also supported a high rate of 40 C and stable cycling of 700 cycles with 70% capacity retention. Akin to Fe, the manganese element is also Earth-abundant and low-cost, which is attractive for ASIB applications. Later, Feng et al. constructed another

ASIB full cell based on a $Na_2Zn_3[Fe(CN)_6]$ cathode, a layer-structured $Na_3Fe_3(PO_4)_4$ anode, and concentrated electrolytes [100]. The full cell reaction can be expressed as:

$$Na_2Zn_3[Fe^{II}(CN)_6]_2 + Na_3Fe^{III}{}_3(PO_4)_4 \leftrightarrow Zn_3[Fe^{III}(CN)_6]_2 + Na_5Fe^{III}Fe^{II}{}_2(PO_4)_4.$$

This full cell gave a promising voltage of ~1.2 V (Figure 8b), a high energy density of ~46 Wh kg^{-1}, an ultra-high rate of 200 C, and long cycling of 3000 cycles. Such a performance greatly exceeded previously reported Fe-based ASIBs, indicating the promise of combining a PBA cathode and a phosphate anode.

5. Summary and Outlook

Fe-based ASIBs are appealing for stationary energy storage, due to the desirable combination of Na/Fe elements and aqueous electrolytes. Therefore, low cost, high sustainability, and high safety can be expected. Here, we suggest some directions to further improve ASIB performance (Table 1).

Table 1. Electrochemical properties of typical iron-based cathode and anode materials.

Material	Potential (V) vs. SHE	Capacity (mAh g^{-1})	Rate Performance	Capacity Retention	Refs.
Olivine $NaFePO_4$	−0.01 V	70 at 0.2 C	38.5 at 2 C	79% after 35 cycles at 0.2 C	[70]
Olivine $NaFePO_4$@AlF_3	0.05 V	95.6 at 1 C	52 at 2 C	58.4% after 50 cycles at 1 C	[71]
$Na_2FeP_2O_7$	0.25 V	65 at 0.2 C	37 at 10 C	86% after 300 cycles at 1 C	[78]
$Na_2FeP_2O_7$-CT	0.29 V	78 at 0.2 mA cm^{-2}	58 at 2 mA cm^{-2}	89% after 30 cycles at 2 mA cm^{-2}	[79]
$Na_4Fe_3(PO_4)_2P_2O_7$	0.30 V	84 at 1 C	N/A	74% in 50 cycles at 1 C	[81]
Na_2FePO_4F	0.31 V	84 at 1 mA cm^{-2}	75 at 5 mA cm^{-2}	93% after 100 cycles at 1 mA cm^{-2}	[83]
$Na_3FePO_4CO_3$	0.56 V	78.6 at 0.2 C	40 at 2 C	N/A	[85]
$Fe[Fe(CN)_6]_{0.87}\cdot\square_{0.13}$	0.397 V	125 at 2 C	102 at 20 C	83% after 500 cycles at 10 C	[21]
$FeFe(CN)_6$	0.297 V	118 at 400 mA g^{-1}	96 at 700 mA g^{-1}	94% after 400 cycles at 700 mA g^{-1}	[97]
$Na_{0.75}Fe_{1.08}[Fe(CN)_6]\cdot 3.5H_2O$	0.44 V	65 at 0.2 C	26 at 10 C	97% after 50 cycles at 1 C	[98]
PB-Na	0.6 V	126.2 at 1 A g^{-1}	53.8 at 10 A g^{-1}	65.1% after 17,000 cycles at 2 A g^{-1}	[99]
$Fe_4[Fe(CN)_6]_3$	0.442 V	107 at 0.5 A g^{-1}	33 at 5 A g^{-1}	Minimal fading after 1100 cycles	[100]
$Na_xFeFe(CN)_6$-$N_{0.23}$	0.392 V	105.9 at 200 mA g^{-1}	45.8 at 3000 mA g^{-1}	73.1% after 1000 cycles at 1000 mA g^{-1}	[101]
$FePO_4\cdot 2H_2O$	0 V	80 at 0.5 C	60 at 6 C	88% after 200 cycles at 1 C	[104]
NASICON-type $Na_3Fe_2(PO_4)_3$	0 V	60.2 at 1 C	36 at 100 C	61% after 1000 cycles at 100 C	[105]
Layer-structured $Na_3Fe_3(PO_4)_4$	−0.2 V	80	42 at 200 C	72% over 6000 cycles at 10 C	[106]
Nano-sized α-Fe_2O_3 spheres	−0.75 V	18 at 0.1 A g^{-1}	N/A	73% after 1000 GCD cycles at 2 A g^{-1}	[108]
Fe_3O_4@rGO	−1.0 V	64 at 1 mA cm^{-2}	N/A	90% over 1000 cycles at 8 mA cm^{-2}	[110]
rGo@C/Fe_3C	−0.6 V	95.3 at 1 A g^{-1}	66.5% at 20 A g^{-1}	81.5% after 5000 cycles 10 A g^{-1}	[112]
FeS_2@rGO	−0.35 V	100	N/A	72.2% after 100 cycles	[114]

Regarding cathodes, we believe $Na_4Fe_3(PO_4)_2P_2O_7$ and $Na_2Fe[Fe(CN)]_6$ materials are competitive candidates, due to their high potentials, high capacities, and easy synthesis. Currently, their cycling performance is not particularly long, but it could be further improved by using concentrated electrolytes or surface coating, which can effectively suppress electrode–electrolyte side reactions and material dissolution. Regarding anodes, sodium iron phosphates are more promising than iron oxides, carbides, or selenides. Currently, $Na_3Fe_2(PO_4)_3$ and $Na_3Fe_3(PO_4)_4$ materials have shown encouraging performance in concentrated electrolytes, which may be further boosted if surface coating is used, or artificial solid-electrolyte interphase (SEI) can be formed. Moreover, we emphasize that there are many other iron phosphate materials in non-aqueous SIBs, which need extensive examination in aqueous electrolytes.

On the full cell level, more research efforts are required to demonstrate the efficacy of all-iron-based ASIB full cells. Currently, there are limited publications in this direction, and the performance of these cells is sub-optimal. For potential commercialization, aqueous Na-ion full cells should exhibit competitive properties (energy, cycling, price, etc.) compared with existing aqueous batteries, especially lead-acid batteries [116]. Lead-acid batteries exhibit an energy density of ~30 Wh kg^{-1}, which is based on the entire mass of the battery system. However, the current ASIB studies only consider the active mass for academic research purposes. Moreover, most studies use a high current rate to demonstrate long cycling, which should also be realized at a low current rate. To further decrease the battery price, low-cost and anti-corrosive current collectors and electrolytes should be developed.

In summary, the development of advanced Fe-based ASIBs warrants the holistic design of cathode materials, anode materials, electrolytes, and full cells. Different approaches should be considered and compared, such as the carbon coating, surface modification, electrolyte design, and pouch cell assembly, to demonstrate more practical Fe-based Na-ion full cells. We hope this review can provide an overall picture of the research status of aqueous Na-ion batteries, and that it will motivate researchers to develop more effective strategies to expediate ASIB research and development. If successful, ASIBs will play an important role in stationary energy storage and contribute to the use of renewable energy sources.

Author Contributions: Conceptualization, Z.F. and X.W.; investigation, S.C. and S.Q; data curation, S.C., S.Q., S.K. and J.F.F.G.; writing—original draft preparation, S.C., S.Q., S.K. and J.F.F.G.; writing—review and editing, Z.F. and X.W.; supervision, Z.F. and X.W.; funding acquisition, Z.F. and X.W. All authors have read and agreed to the published version of the manuscript.

Funding: Z.F. (Zhenxing Feng) acknowledges financial support from the U.S. National Science Foundation (award numbers: CBET-2016192 and CBET-1949870) and the Oregon Metal Initiative. X.W. acknowledges support from NSF Center for the Advancement of Wearable Technologies (No. 1849243).

Data Availability Statement: This paper contains no supporting data.

Conflicts of Interest: The authors declare no conflict of interest.

References

1. Yang, Z.; Zhang, J.; Kintner-Meyer, M.C.W.; Lu, X.; Choi, D.; Lemmon, J.P.; Liu, J. Electrochemical energy storage for green grid. *Chem. Rev.* **2011**, *111*, 3577–3613. [CrossRef]
2. Liu, J.; Xiao, J.; Yang, J.; Wang, W.; Shao, Y.; Liu, P.; Whittingham, M.S. The TWh challenge: Next generation batteries for energy storage and electric vehicles. *Next Energy* **2023**, *1*, 100015. [CrossRef]
3. Li, M.; Lu, J.; Chen, Z.; Amine, K. 30 years of lithium-ion batteries. *Adv. Mater.* **2018**, *30*, 1800561. [CrossRef] [PubMed]
4. Manthiram, A. An outlook on lithium ion battery technology. *ACS Cent. Sci.* **2017**, *3*, 1063–1069. [CrossRef]
5. Tarascon, J.-M. Is lithium the new gold? *Nat. Chem.* **2010**, *2*, 510. [CrossRef]
6. Murdock, B.E.; Toghill, K.E.; Tapia-Ruiz, N. A perspective on the sustainability of cathode materials used in lithium-ion batteries. *Adv. Energy Mater.* **2021**, *11*, 2102028. [CrossRef]
7. Von Wald Cresce, A.; Xu, K. Aqueous lithium-ion batteries. *Carbon Energy* **2021**, *3*, 721–751. [CrossRef]
8. Yabuuchi, N.; Kubota, K.; Dahbi, M.; Komaba, S. Research development on sodium-ion batteries. *Chem. Rev.* **2014**, *114*, 11636–11682. [CrossRef] [PubMed]
9. Hwang, J.-Y.; Myung, S.-T.; Sun, Y.-K. Sodium-ion batteries: Present and future. *Chem. Soc. Rev.* **2017**, *46*, 3529–3614. [CrossRef] [PubMed]
10. Vaalma, C.; Buchholz, D.; Weil, M.; Passerini, S. A cost and resource analysis of sodium-ion batteries. *Nat. Rev. Mater.* **2018**, *3*, 18013. [CrossRef]
11. Chayambuka, K.; Mulder, G.; Danilov, D.L.; Notten, P.H.L. Sodium-ion battery materials and electrochemical properties reviewed. *Adv. Energy Mater.* **2018**, *8*, 1800079. [CrossRef]
12. Nayak, P.K.; Yang, L.; Brehm, W.; Adelhelm, P. From lithium-ion to sodium-ion batteries: Advantages, challenges, and surprises. *Angew. Chem. Int. Ed.* **2018**, *57*, 102–120. [CrossRef] [PubMed]
13. Qian, J.; Chen, Y.; Wu, L.; Cao, Y.; Ai, X.; Yang, H. High capacity Na-storage and superior cyclability of nanocomposite Sb/C anode for Na-ion batteries. *Chem. Commun.* **2012**, *48*, 7070–7072. [CrossRef] [PubMed]
14. Qian, J.; Wu, X.; Cao, Y.; Ai, X.; Yang, H. High capacity and rate capability of amorphous phosphorus for sodium ion batteries. *Angew. Chem.* **2013**, *125*, 4731–4734. [CrossRef]

15. Pan, H.; Hu, Y.-S.; Chen, L. Room-temperature stationary sodium-ion batteries for large-scale electric energy storage. *Energy Environ. Sci.* **2013**, *6*, 2338–2360. [CrossRef]
16. Komaba, S.; Itabashi, T.; Watanabe, M.; Groult, H.; Kumagai, N. Electrochemistry of graphite in Li and Na salt codissolving electrolyte for rechargeable batteries. *J. Electrochem. Soc.* **2007**, *154*, A322. [CrossRef]
17. Kubota, K.; Yabuuchi, N.; Yoshida, H.; Dahbi, M.; Komaba, S. Layered oxides as positive electrode materials for Na-ion batteries. *MRS Bull.* **2014**, *39*, 416–422. [CrossRef]
18. Wang, Y.; Yu, X.; Xu, S.; Bai, J.; Xiao, R.; Hu, Y.-S.; Li, H.; Yang, X.-Q.; Chen, L.; Huang, X. A zero-strain layered metal oxide as the negative electrode for long-life sodium-ion batteries. *Nat. Commun.* **2013**, *4*, 2365. [CrossRef]
19. Mu, L.-Q.; Hu, Y.-S.; Chen, L.-Q. New layered metal oxides as positive electrode materials for room-temperature sodium-ion batteries. *Chin. Phys. B* **2015**, *24*, 038202. [CrossRef]
20. Qian, J.; Wu, C.; Cao, Y.; Ma, Z.; Huang, Y.; Ai, X.; Yang, H. Prussian blue cathode materials for sodium-ion batteries and other ion batteries. *Adv. Energy Mater.* **2018**, *8*, 1702619. [CrossRef]
21. Wu, X.; Luo, Y.; Sun, M.; Qian, J.; Cao, Y.; Ai, X.; Yang, H. Low-defect Prussian blue nanocubes as high capacity and long life cathodes for aqueous Na-ion batteries. *Nano Energy* **2015**, *13*, 117–123. [CrossRef]
22. Wu, X.; Sun, M.; Guo, S.; Qian, J.; Liu, Y.; Cao, Y.; Ai, X.; Yang, H. Vacancy-free Prussian blue nanocrystals with high capacity and superior cyclability for aqueous sodium-ion batteries. *ChemNanoMat* **2015**, *1*, 188–193. [CrossRef]
23. Fang, Y.; Zhang, J.; Xiao, L.; Ai, X.; Cao, Y.; Yang, H. Phosphate framework electrode materials for sodium ion batteries. *Adv. Sci.* **2017**, *4*, 1600392. [CrossRef] [PubMed]
24. Zeng, Z.; Jiang, X.; Li, R.; Yuan, D.; Ai, X.; Yang, H.; Cao, Y. A safer sodium-ion battery based on nonflammable organic phosphate electrolyte. *Adv. Sci.* **2016**, *3*, 1600066. [CrossRef]
25. Liu, X.; Jiang, X.; Zhong, F.; Feng, X.; Chen, W.; Ai, X.; Yang, H.; Cao, Y. High-safety symmetric sodium-ion batteries based on nonflammable phosphate electrolyte and double $Na_3V_2(PO_4)_3$ electrodes. *ACS Appl. Mater. Interfaces* **2019**, *11*, 27833–27838. [CrossRef]
26. Xiao, L.; Lu, H.; Fang, Y.; Sushko, M.L.; Cao, Y.; Ai, X.; Yang, H.; Liu, J. Low-defect and low-porosity hard carbon with high coulombic efficiency and high capacity for practical sodium ion battery anode. *Adv. Energy Mater.* **2018**, *8*, 1703238. [CrossRef]
27. Xiao, L.; Cao, Y.; Henderson, W.A.; Sushko, M.L.; Shao, Y.; Xiao, J.; Wang, W.; Engelhard, M.H.; Nie, Z.; Liu, J. Hard carbon nanoparticles as high-capacity, high-stability anodic materials for Na-ion batteries. *Nano Energy* **2016**, *19*, 279–288. [CrossRef]
28. Li, Z.; Jian, Z.; Wang, X.; Rodríguez-Pérez, I.A.; Bommier, C.; Ji, X. Hard carbon anodes of sodium-ion batteries: Undervalued rate capability. *Chem. Commun.* **2017**, *53*, 2610–2613. [CrossRef]
29. Bommier, C.; Surta, T.W.; Dolgos, M.; Ji, X. New mechanistic insights on Na-ion storage in nongraphitizable carbon. *Nano Lett.* **2015**, *15*, 5888–5892. [CrossRef]
30. Deng, J.; Luo, W.B.; Chou, S.L.; Liu, H.K.; Dou, S.X. Sodium-ion batteries: From academic research to practical commercialization. *Adv. Energy Mater.* **2018**, *8*, 1701428. [CrossRef]
31. Zhang, M.; Li, Y.; Wu, F.; Bai, Y.; Wu, C. Boost sodium-ion batteries to commercialization: Strategies to enhance initial Coulombic efficiency of hard carbon anode. *Nano Energy* **2021**, *82*, 105738. [CrossRef]
32. Liu, Q.; Hu, Z.; Chen, M.; Zou, C.; Jin, H.; Wang, S.; Chou, S.L.; Liu, Y.; Dou, S.X. The cathode choice for commercialization of sodium-ion batteries: Layered transition metal oxides versus Prussian blue analogs. *Adv. Funct. Mater.* **2020**, *30*, 1909530. [CrossRef]
33. Bauer, A.; Song, J.; Vail, S.; Pan, W.; Barker, J.; Lu, Y. The scale-up and commercialization of nonaqueous Na-ion battery technologies. *Adv. Energy Mater.* **2018**, *8*, 1702869. [CrossRef]
34. Ponrouch, A.; Monti, D.; Boschin, A.; Steen, B.; Johansson, P.; Palacín, M.R. Non-aqueous electrolytes for sodium-ion batteries. *J. Mater. Chem. A* **2015**, *3*, 22–42. [CrossRef]
35. Li, Z.; Young, D.; Xiang, K.; Carter, W.C.; Chiang, Y.M. Towards high power high energy aqueous sodium-ion batteries: The $NaTi_2(PO_4)_3/Na_{0.44}MnO_2$ system. *Adv. Energy Mater.* **2013**, *3*, 290–294. [CrossRef]
36. Whitacre, J.F.; Tevar, A.; Sharma, S. Na4Mn9O18 as a positive electrode material for an aqueous electrolyte sodium-ion energy storage device. *Electrochem. Commun.* **2010**, *12*, 463–466. [CrossRef]
37. Wu, X.; Cao, Y.; Ai, X.; Qian, J.; Yang, H. A low-cost and environmentally benign aqueous rechargeable sodium-ion battery based on $NaTi_2(PO_4)_3$–$Na_2NiFe(CN)_6$ intercalation chemistry. *Electrochem. Commun.* **2013**, *31*, 145–148. [CrossRef]
38. Bin, D.; Wang, F.; Tamirat, A.G.; Suo, L.; Wang, Y.; Wang, C.; Xia, Y. Progress in aqueous rechargeable sodium-ion batteries. *Adv. Energy Mater.* **2018**, *8*, 1703008. [CrossRef]
39. Wang, Y.; Yi, J.; Xia, Y. Recent progress in aqueous lithium-ion batteries. *Adv. Energy Mater.* **2012**, *2*, 830–840. [CrossRef]
40. Sui, Y.; Ji, X. Anticatalytic strategies to suppress water electrolysis in aqueous batteries. *Chem. Rev.* **2021**, *121*, 6654–6695. [CrossRef]
41. Suo, L.; Borodin, O.; Gao, T.; Olguin, M.; Ho, J.; Fan, X.; Luo, C.; Wang, C.; Xu, K. "Water-in-salt" electrolyte enables high-voltage aqueous lithium-ion chemistries. *Science* **2015**, *350*, 938–943. [CrossRef] [PubMed]
42. Jiang, L.; Liu, L.; Yue, J.; Zhang, Q.; Zhou, A.; Borodin, O.; Suo, L.; Li, H.; Chen, L.; Xu, K.; et al. High-voltage aqueous Na-ion battery enabled by inert-cation-assisted water-in-salt electrolyte. *Adv. Mater.* **2020**, *32*, 1904427. [CrossRef] [PubMed]
43. Wu, X.; Xu, Y.; Zhang, C.; Leonard, D.P.; Markir, A.; Lu, J.; Ji, X. Reverse dual-ion battery via a $ZnCl_2$ water-in-salt electrolyte. *J. Am. Chem. Soc.* **2019**, *141*, 6338–6344. [CrossRef]

44. Suo, L.; Borodin, O.; Wang, Y.; Rong, X.; Sun, W.; Fan, X.; Xu, S.; Schroeder, M.A.; Cresce, A.V.; Wang, F. "Water-in-salt" electrolyte makes aqueous sodium-ion battery safe, green, and long-lasting. *Adv. Energy Mater.* **2017**, *7*, 1701189. [CrossRef]
45. Jin, T.; Ji, X.; Wang, P.F.; Zhu, K.; Zhang, J.; Cao, L.; Chen, L.; Cui, C.; Deng, T.; Liu, S.; et al. High-Energy Aqueous Sodium-Ion Batteries. *Angew. Chem. Int. Ed.* **2021**, *60*, 11943–11948. [CrossRef]
46. Gheytani, S.; Liang, Y.; Wu, F.; Jing, Y.; Dong, H.; Rao, K.K.; Chi, X.; Fang, F.; Yao, Y. An aqueous Ca-ion battery. *Adv. Sci.* **2017**, *4*, 1700465. [CrossRef]
47. Chen, L.; Bao, J.L.; Dong, X.; Truhlar, D.G.; Wang, Y.; Wang, C.; Xia, Y. Aqueous Mg-ion battery based on polyimide anode and prussian blue cathode. *ACS Energy Lett.* **2017**, *2*, 1115–1121. [CrossRef]
48. Yan, C.; Lv, C.; Wang, L.; Cui, W.; Zhang, L.; Dinh, K.N.; Tan, H.; Wu, C.; Wu, T.; Ren, Y. Architecting a stable high-energy aqueous Al-ion battery. *J. Am. Chem. Soc.* **2020**, *142*, 15295–15304. [CrossRef] [PubMed]
49. Li, Y.; Deng, W.; Zhou, Z.; Li, C.; Zhang, M.; Yuan, X.; Hu, J.; Chen, H.; Li, R. An ultra-long life aqueous full K-ion battery. *J. Mater. Chem. A* **2021**, *9*, 2822–2829. [CrossRef]
50. Wen, X.; Luo, J.; Xiang, K.; Zhou, W.; Zhang, C.; Chen, H. High-performance monoclinic WO_3 nanospheres with the novel NH_4^+ diffusion behaviors for aqueous ammonium-ion batteries. *Chem. Eng. J.* **2023**, *458*, 141381. [CrossRef]
51. Available online: https://en.wikipedia.org/wiki/Aquion_Energy (accessed on 26 April 2023).
52. Pang, G.; Nie, P.; Yuan, C.; Shen, L.; Zhang, X.; Zhu, J.; Ding, B. Enhanced Performance of Aqueous Sodium-Ion Batteries Using Electrodes Based on the $NaTi_2(PO_4)_3$/MWNTs–$Na_{0.44}MnO_2$ System. *Energy Technol.* **2014**, *2*, 705–712. [CrossRef]
53. Kim, D.J.; Ponraj, R.; Kannan, A.G.; Lee, H.-W.; Fathi, R.; Ruffo, R.; Mari, C.M.; Kim, D.K. Diffusion behavior of sodium ions in $Na_{0.44}MnO_2$ in aqueous and non-aqueous electrolytes. *J. Power Source* **2013**, *244*, 758–763. [CrossRef]
54. Shen, X.; Han, M.; Li, X.; Zhang, P.; Yang, C.; Liu, H.; Hu, Y.-S.; Zhao, J. Regulated Synthesis of α-$NaVOPO_4$ with an Enhanced Conductive Network as a High-Performance Cathode for Aqueous Na-Ion Batteries. *ACS Appl. Mater. Interfaces* **2022**, *14*, 6841–6851. [CrossRef] [PubMed]
55. Hung, T.-F.; Lan, W.-H.; Yeh, Y.-W.; Chang, W.-S.; Yang, C.-C.; Lin, J.-C. Hydrothermal synthesis of sodium titanium phosphate nanoparticles as efficient anode materials for aqueous sodium-ion batteries. *ACS Sustain. Chem. Eng.* **2016**, *4*, 7074–7079. [CrossRef]
56. Guo, X.; Wang, Z.; Deng, Z.; Li, X.; Wang, B.; Chen, X.; Ong, S.P. Water contributes to higher energy density and cycling stability of Prussian blue analogue cathodes for aqueous sodium-ion batteries. *Chem. Mater.* **2019**, *31*, 5933–5942. [CrossRef]
57. Wessells, C.D.; Peddada, S.V.; Huggins, R.A.; Cui, Y. Nickel hexacyanoferrate nanoparticle electrodes for aqueous sodium and potassium ion batteries. *Nano Lett.* **2011**, *11*, 5421–5425. [CrossRef]
58. Deng, W.; Shen, Y.; Qian, J.; Yang, H. A polyimide anode with high capacity and superior cyclability for aqueous Na-ion batteries. *Chem. Commun.* **2015**, *51*, 5097–5099. [CrossRef]
59. Available online: https://en.wikipedia.org/wiki/Abundance_of_the_chemical_elements (accessed on 9 June 2023).
60. Available online: https://en.wikipedia.org/wiki/Prices_of_chemical_elements (accessed on 16 May 2023).
61. Fang, Y.; Chen, Z.; Xiao, L.; Ai, X.; Cao, Y.; Yang, H. Recent progress in iron-based electrode materials for grid-scale sodium-ion batteries. *Small* **2018**, *14*, 1703116. [CrossRef]
62. Okada, S.; Yamaki, J.-I. Iron-based cathodes/anodes for Li-ion and post Li-ion batteries. *J. Ind. Eng. Chem.* **2004**, *10*, 1104–1113.
63. Liu, Y.; Li, W.; Xia, Y. Recent progress in polyanionic anode materials for Li(Na)-ion batteries. *Electrochem. Energy Rev.* **2021**, *4*, 447–472. [CrossRef]
64. Padhi, A.K.; Nanjundaswamy, K.S.; Goodenough, J.B. Phospho-olivines as positive-electrode materials for rechargeable lithium batteries. *J. Electrochem. Soc.* **1997**, *144*, 1188. [CrossRef]
65. Sun, C.; Rajasekhara, S.; Goodenough, J.B.; Zhou, F. Monodisperse porous $LiFePO_4$ microspheres for a high power Li-ion battery cathode. *J. Am. Chem. Soc.* **2011**, *133*, 2132–2135. [CrossRef]
66. Fang, Y.; Liu, Q.; Xiao, L.; Ai, X.; Yang, H.; Cao, Y. High-performance olivine $NaFePO_4$ microsphere cathode synthesized by aqueous electrochemical displacement method for sodium ion batteries. *ACS Appl. Mater. Interfaces* **2015**, *7*, 17977–17984. [CrossRef] [PubMed]
67. Avdeev, M.; Mohamed, Z.; Ling, C.D.; Lu, J.; Tamaru, M.; Yamada, A.; Barpanda, P. Magnetic structures of $NaFePO_4$ maricite and triphylite polymorphs for sodium-ion batteries. *Inorg. Chem.* **2013**, *52*, 8685–8693. [CrossRef]
68. Kim, J.; Seo, D.-H.; Kim, H.; Park, I.; Yoo, J.-K.; Jung, S.-K.; Park, Y.-U.; Goddard Iii, W.A.; Kang, K. Unexpected discovery of low-cost maricite $NaFePO_4$ as a high-performance electrode for Na-ion batteries. *Energy Environ. Sci.* **2015**, *8*, 540–545. [CrossRef]
69. Vujković, M.; Mentus, S. Fast sodiation/desodiation reactions of electrochemically delithiated olivine $LiFePO_4$ in aerated aqueous $NaNO_3$ solution. *J. Power Source* **2014**, *247*, 184–188. [CrossRef]
70. Fernández-Ropero, A.J.; Saurel, D.; Acebedo, B.; Rojo, T.; Casas-Cabanas, M. Electrochemical characterization of $NaFePO_4$ as positive electrode in aqueous sodium-ion batteries. *J. Power Source* **2015**, *291*, 40–45. [CrossRef]
71. Jeong, S.; Kim, B.H.; Park, Y.D.; Lee, C.Y.; Mun, J.; Tron, A. Artificially coated $NaFePO_4$ for aqueous rechargeable sodium-ion batteries. *J. Alloys Compd.* **2019**, *784*, 720–726. [CrossRef]
72. Tang, W.; Song, X.; Du, Y.; Peng, C.; Lin, M.; Xi, S.; Tian, B.; Zheng, J.; Wu, Y.; Pan, F. High-performance $NaFePO_4$ formed by aqueous ion-exchange and its mechanism for advanced sodium ion batteries. *J. Mater. Chem. A* **2016**, *4*, 4882–4892. [CrossRef]
73. Song, X.; Liu, T.; Amine, J.; Duan, Y.; Zheng, J.; Lin, Y.; Pan, F. In-situ mass-electrochemical study of surface redox potential and interfacial chemical reactions of Li (Na) $FePO_4$ nanocrystals for Li (Na)-ion batteries. *Nano Energy* **2017**, *37*, 90–97. [CrossRef]

74. Sevinc, S.; Tekin, B.; Ata, A.; Morcrette, M.; Perrot, H.; Sel, O.; Demir-Cakan, R. In-situ tracking of $NaFePO_4$ formation in aqueous electrolytes and its electrochemical performances in Na-ion/polysulfide batteries. *J. Power Source* **2019**, *412*, 55–62. [CrossRef]
75. Shiprath, K.; Manjunatha, H.; Ratnamala, A.; Ramesh, S.; Naidu, K.C.B. Electrochemical Study of $NaFePO_4$ Cathode Material in Aqueous Sodium-ion Electrolyte. *Biointerface Res. Appl. Chem.* **2021**, *13*, 186.
76. Barpanda, P.; Liu, G.; Ling, C.D.; Tamaru, M.; Avdeev, M.; Chung, S.-C.; Yamada, Y.; Yamada, A. $Na_2FeP_2O_7$: A safe cathode for rechargeable sodium-ion batteries. *Chem. Mater.* **2013**, *25*, 3480–3487. [CrossRef]
77. Kim, H.; Shakoor, R.A.; Park, C.; Lim, S.Y.; Kim, J.S.; Jo, Y.N.; Cho, W.; Miyasaka, K.; Kahraman, R.; Jung, Y. $Na_2FeP_2O_7$ as a promising iron-based pyrophosphate cathode for sodium rechargeable batteries: A combined experimental and theoretical study. *Adv. Funct. Mater.* **2013**, *23*, 1147–1155. [CrossRef]
78. Jung, Y.H.; Lim, C.H.; Kim, J.-H.; Kim, D.K. $Na_2FeP_2O_7$ as a positive electrode material for rechargeable aqueous sodium-ion batteries. *RSC Adv.* **2014**, *4*, 9799–9802. [CrossRef]
79. Nakamoto, K.; Kano, Y.; Kitajou, A.; Okada, S. Electrolyte dependence of the performance of a $Na_2FeP_2O_7//NaTi_2(PO_4)_3$ rechargeable aqueous sodium-ion battery. *J. Power Source* **2016**, *327*, 327–332. [CrossRef]
80. Pu, X.; Wang, H.; Yuan, T.; Cao, S.; Liu, S.; Xu, L.; Yang, H.; Ai, X.; Chen, Z.; Cao, Y. $Na_4Fe_3(PO_4)\ _2P_2O_7$/C nanospheres as low-cost, high-performance cathode material for sodium-ion batteries. *Energy Storage Mater.* **2019**, *22*, 330–336. [CrossRef]
81. Fernández-Ropero, A.J.; Zarrabeitia, M.; Reynaud, M.; Rojo, T.; Casas-Cabanas, M. Toward safe and sustainable batteries: $Na_4Fe_3(PO_4)_2P_2O_7$ as a low-cost cathode for rechargeable aqueous Na-ion batteries. *J. Phys. Chem. C* **2018**, *122*, 133–142. [CrossRef]
82. Kawabe, Y.; Yabuuchi, N.; Kajiyama, M.; Fukuhara, N.; Inamasu, T.; Okuyama, R.; Nakai, I.; Komaba, S. Synthesis and electrode performance of carbon coated Na_2FePO_4F for rechargeable Na batteries. *Electrochem. Commun.* **2011**, *13*, 1225–1228. [CrossRef]
83. Sharma, L.; Nakamoto, K.; Sakamoto, R.; Okada, S.; Barpanda, P. Na_2FePO_4F Fluorophosphate as Positive Insertion Material for Aqueous Sodium-Ion Batteries. *ChemElectroChem* **2019**, *6*, 444–449. [CrossRef]
84. Xie, B.; Sakamoto, R.; Kitajou, A.; Nakamoto, K.; Zhao, L.; Okada, S.; Fujita, Y.; Oka, N.; Nishida, T.; Kobayashi, W. Cathode properties of $Na_3FePO_4CO_3$ prepared by the mechanical ball milling method for Na-ion batteries. *Sci. Rep.* **2020**, *10*, 3278. [CrossRef] [PubMed]
85. Shiprath, K.; Manjunatha, H.; Ratnam, K.V.; Janardan, S. Synthesis of Flower-Like, Hyperbranched $Na_3FePO_4CO_3$ Nanocrystals and Their Electrochemical Performance as Cathodes in Aqueous Rechargeable Sodium-Ion Batteries. *J. Electrochem. Soc.* **2021**, *168*, 080523. [CrossRef]
86. Herren, F.; Fischer, P.; Ludi, A.; Hälg, W. Neutron diffraction study of Prussian Blue, $Fe_4[Fe(CN)_6]_3$. xH_2O. Location of water molecules and long-range magnetic order. *Inorg. Chem.* **1980**, *19*, 956–959. [CrossRef]
87. You, Y.; Wu, X.-L.; Yin, Y.-X.; Guo, Y.-G. High-quality Prussian blue crystals as superior cathode materials for room-temperature sodium-ion batteries. *Energy Environ. Sci.* **2014**, *7*, 1643–1647. [CrossRef]
88. Wessells, C.D.; Peddada, S.V.; McDowell, M.T.; Huggins, R.A.; Cui, Y. The effect of insertion species on nanostructured open framework hexacyanoferrate battery electrodes. *J. Electrochem. Soc.* **2011**, *159*, A98. [CrossRef]
89. Wessells, C.D.; Huggins, R.A.; Cui, Y. Copper hexacyanoferrate battery electrodes with long cycle life and high power. *Nat. Commun.* **2011**, *2*, 550. [CrossRef]
90. Li, Y.; Zhao, J.; Hu, Q.; Hao, T.; Cao, H.; Huang, X.; Liu, Y.; Zhang, Y.; Lin, D.; Tang, Y. Prussian blue analogs cathodes for aqueous zinc ion batteries. *Mater. Today Energy* **2022**, *29*, 101095. [CrossRef]
91. Du, G.; Pang, H. Recent advancements in Prussian blue analogues: Preparation and application in batteries. *Energy Storage Mater.* **2021**, *36*, 387–408. [CrossRef]
92. Hurlbutt, K.; Wheeler, S.; Capone, I.; Pasta, M. Prussian blue analogs as battery materials. *Joule* **2018**, *2*, 1950–1960. [CrossRef]
93. Qiu, S.; Xu, Y.; Wu, X.; Ji, X. Prussian blue analogues as electrodes for aqueous monovalent ion batteries. *Electrochem. Energy Rev.* **2022**, *5*, 242–262. [CrossRef]
94. Wu, X.; Shao, M.; Wu, C.; Qian, J.; Cao, Y.; Ai, X.; Yang, H. Low defect $FeFe(CN)_6$ framework as stable host material for high performance Li-ion batteries. *ACS Appl. Mater. Interfaces* **2016**, *8*, 23706–23712. [CrossRef] [PubMed]
95. Wu, X.; Deng, W.; Qian, J.; Cao, Y.; Ai, X.; Yang, H. Single-crystal $FeFe(CN)_6$ nanoparticles: A high capacity and high rate cathode for Na-ion batteries. *J. Mater. Chem. A* **2013**, *1*, 10130–10134. [CrossRef]
96. Wu, X.; Wu, C.; Wei, C.; Hu, L.; Qian, J.; Cao, Y.; Ai, X.; Wang, J.; Yang, H. Highly crystallized $Na_2CoFe(CN)_6$ with suppressed lattice defects as superior cathode material for sodium-ion batteries. *ACS Appl. Mater. Interfaces* **2016**, *8*, 5393–5399. [CrossRef]
97. Yang, Q.; Wang, W.; Li, H.; Zhang, J.; Kang, F.; Li, B. Investigation of iron hexacyanoferrate as a high rate cathode for aqueous batteries: Sodium-ion batteries and lithium-ion batteries. *Electrochim. Acta* **2018**, *270*, 96–103. [CrossRef]
98. Fernández-Ropero, A.J.; Piernas-Muñoz, M.J.; Castillo-Martínez, E.; Rojo, T.; Casas-Cabanas, M. Electrochemical characterization of $NaFe_2(CN)_6$ Prussian blue as positive electrode for aqueous sodium-ion batteries. *Electrochim. Acta* **2016**, *210*, 352–357. [CrossRef]
99. Bi, H.; Luo, Y.; Zhao, C.; Ma, L.; Huang, H. Graphene oxide suspension-based electrolyte promotes the cycling performance of aqueous sodium-ion batteries through the interaction between metal ions, free water molecules and functional groups. *J. Power Source* **2023**, *555*, 232380. [CrossRef]
100. Zhou, L.; Yang, Z.; Li, C.; Chen, B.; Wang, Y.; Fu, L.; Zhu, Y.; Liu, X.; Wu, Y. Prussian blue as positive electrode material for aqueous sodium-ion capacitor with excellent performance. *RSC Adv.* **2016**, *6*, 109340–109345. [CrossRef]

101. Wang, J.; Mi, C.; Nie, P.; Dong, S.; Tang, S.; Zhang, X. Sodium-rich iron hexacyanoferrate with nickel doping as a high performance cathode for aqueous sodium ion batteries. *J. Electroanal. Chem.* **2018**, *818*, 10–18. [CrossRef]
102. Park, S.I.; Gocheva, I.; Okada, S.; Yamaki, J.-I. Electrochemical properties of $NaTi_2(PO_4)_3$ anode for rechargeable aqueous sodium-ion batteries. *J. Electrochem. Soc.* **2011**, *158*, A1067. [CrossRef]
103. He, L.; Li, H.; Ge, X.; Li, S.; Wang, X.; Wang, S.; Zhang, L.; Zhang, Z. Iron-Phosphate-Based Cathode Materials for Cost-Effective Sodium-Ion Batteries: Development, Challenges, and Prospects. *Adv. Mater. Interfaces* **2022**, *9*, 2200515. [CrossRef]
104. Wang, Y.; Feng, Z.; Laul, D.; Zhu, W.; Provencher, M.; Trudeau, M.L.; Guerfi, A.; Zaghib, K. Ultra-low cost and highly stable hydrated $FePO_4$ anodes for aqueous sodium-ion battery. *J. Power Source* **2018**, *374*, 211–216. [CrossRef]
105. Qiu, S.; Wu, X.; Wang, M.; Lucero, M.; Wang, Y.; Wang, J.; Yang, Z.; Xu, W.; Wang, Q.; Gu, M.; et al. NASICON-type $Na_3Fe_2(PO_4)_3$ as a low-cost and high-rate anode material for aqueous sodium-ion batteries. *Nano Energy* **2019**, *64*, 103941. [CrossRef]
106. Qiu, S.; Lucero, M.; Wu, X.; Wang, Q.; Wang, M.; Wang, Y.; Samarakoon, W.S.; Bolding, M.R.; Yang, Z.; Huang, Y.; et al. Revealing the Fast and Durable Na^+ Insertion Reactions in a Layered $Na_3Fe_3(PO_4)_4$ Anode for Aqueous Na-Ion Batteries. *ACS Mater. Au* **2021**, *2*, 63–71. [CrossRef] [PubMed]
107. Gund, G.S.; Dubal, D.P.; Chodankar, N.R.; Cho, J.Y.; Gomez-Romero, P.; Park, C.; Lokhande, C.D. Low-cost flexible supercapacitors with high-energy density based on nanostructured MnO_2 and Fe_2O_3 thin films directly fabricated onto stainless steel. *Sci. Rep.* **2015**, *5*, 12454. [CrossRef] [PubMed]
108. Nwanya, A.C.; Ndipingwi, M.M.; Ikpo, C.O.; Ezema, F.I.; Iwuoha, E.I.; Maaza, M. Biomass mediated multi layered $NaNi_xCo_{1-x}O_2$ (x= 0.4) and α-Fe_2O_3 nanoparticles for aqueous sodium ion battery. *J. Electroanal. Chem.* **2020**, *858*, 113809. [CrossRef]
109. Lan, P.; Liu, T.; Ji, X.; Cheng, S. Charge storage behavior and reaction mechanism of α-Fe_2O_3 as anodes for aqueous batteries. *J. Alloys Compd.* **2021**, *859*, 157789. [CrossRef]
110. Lu, K.; Li, D.; Gao, X.; Dai, H.; Wang, N.; Ma, H. An advanced aqueous sodium-ion supercapacitor with a manganous hexacyanoferrate cathode and a Fe_3O_4/rGO anode. *J. Mater. Chem. A* **2015**, *3*, 16013–16019. [CrossRef]
111. Li, N.N.; Sheng, Z.M.; Huang, H.; Chang, C.K.; Jia, R.P.; Han, S. Fe_2O_3 nanoparticles encapsulated with N-doped porous graphitic shells approached by oxidizing Fe_3C@C precursor for high-performance sodium-ion batteries. *J. Alloys Compd.* **2019**, *792*, 25–31. [CrossRef]
112. Tan, Q.; Chen, X.; Wan, H.; Zhang, B.; Liu, X.; Li, L.; Wang, C.; Gan, Y.; Liang, P.; Wang, Y. Metal–organic framework-derived high conductivity Fe_3C with porous carbon on graphene as advanced anode materials for aqueous battery-supercapacitor hybrid devices. *J. Power Source* **2020**, *448*, 227403. [CrossRef]
113. Li, X.; Shen, Y.; Kong, D.; Fan, H.; Gao, X.; Cui, Y.; Jiang, T.; Ren, Y.; Cai, T.; Xing, W. Realizing an aqueous sodium-ion battery with a super-high discharge voltage based on a novel $FeSe_2$@rGO anode. *Inorg. Chem. Front.* **2022**, *9*, 1622–1629. [CrossRef]
114. Zhang, J.; Zhang, D.; Niu, F.; Li, X.; Wang, C.; Yang, J. $FeFe(CN)_6$ Nanocubes as a Bipolar Electrode Material in Aqueous Symmetric Sodium-Ion Batteries. *ChemPlusChem* **2017**, *82*, 1170–1173. [CrossRef] [PubMed]
115. Wang, B.; Wang, X.; Liang, C.; Yan, M.; Jiang, Y. An All-Prussian-Blue-Based Aqueous Sodium-Ion Battery. *ChemElectroChem* **2019**, *6*, 4848–4853. [CrossRef]
116. Zhang, Y.; Zhou, C.-G.; Yang, J.; Xue, S.-C.; Gao, H.-L.; Yan, X.-H.; Huo, Q.-Y.; Wang, S.-W.; Cao, Y.; Yan, J. Advances and challenges in improvement of the electrochemical performance for lead-acid batteries: A comprehensive review. *J. Power Source* **2022**, *520*, 230800. [CrossRef]